

Original Article

Cite this article: Alam M, Muguli T, Gurumurthy GP, Arif M, Sohrin Y, Singh AD, Radhakrishna T, Pandey DK, and Verma K (2023) Hydroclimatic conditions and sediment provenance in the northeastern Arabian Sea since the late Miocene: insights from geochemical and environmental magnetic records at IODP Site U1457 of the Laxmi Basin. *Geological Magazine* **160**: 813–829. <https://doi.org/10.1017/S0016756822001273>

Received: 23 May 2022

Revised: 5 December 2022

Accepted: 7 December 2022

First published online: 10 February 2023

Keywords:


Chemical weathering; Indus River Basin; Indian monsoon evolution; Neogene–Pleistocene; Western Himalayas; Northern Indian Ocean

Author for correspondence:

G.P. Gurumurthy,

Email: gurumurthygp@bsip.res.in

Hydroclimatic conditions and sediment provenance in the northeastern Arabian Sea since the late Miocene: insights from geochemical and environmental magnetic records at IODP Site U1457 of the Laxmi Basin

Mahboob Alam^{1,2}, Tripti Muguli³, G.P. Gurumurthy^{1,4} , Mohammad Arif^{1,4}, Yoshiki Sohrin⁵, Arun Deo Singh², T. Radhakrishna⁶, Dhananjai Kumar Pandey⁷ and Komal Verma²

¹Birbal Sahni Institute of Palaeosciences, Lucknow 226007, India; ²Department of Geology, Banaras Hindu University, Varanasi 221005, India; ³National Centre for Earth Science Studies, Ministry of Earth Sciences, Thiruvananthapuram 695011, India; ⁴Academy of Scientific and Innovative Research, CSIR-HRDC Campus, Ghaziabad 201002, India; ⁵Institute for Chemical Research, Kyoto University, Kyoto 6110011, Japan; ⁶GITAM University, Nagadenehalli, Bengaluru 561203, India and ⁷National Centre for Polar and Ocean Research, Ministry of Earth Sciences, Vasco-da-Gama 403804, Goa, India

Abstract

Palaeo-monsoon and palaeoclimate conditions over Southeast Asia are a matter of debate despite notable studies on the continental and oceanic sedimentary record. The present study investigates the environmental magnetic and geochemical records preserved in the deep marine sediments of the northeastern (NE) Arabian Sea to elucidate the erosion history of the western Himalayas and its link with the prevailing hydroclimatic conditions since the late Miocene. For this, the sediment core retrieved during International Ocean Discovery Program (IODP) Expedition 355 at Site U1457 in the NE Arabian Sea has been explored. The results reveal that the hydroclimatic conditions were predominantly arid during the late Miocene, except for humid intervals from 6.1 Ma to 5.6 Ma. Humid climate conditions in the Indus River Basin returned during the mid-Pliocene and continued to the Pleistocene with an intense chemical weathering regime from 1.9 Ma to 1.2 Ma. The dominant sediment source to the NE Arabian Sea at Site U1457 during the late Miocene and the Pliocene was the Indus River, while during the Pleistocene, mixed sediments brought by the Indus River and the Peninsular Indian rivers were observed. The sediment contribution from a chemically less altered mafic source (the Deccan basalts) increased between 1.2 Ma and 0.2 Ma, possibly linked to a weak Indian Summer Monsoon. The summer monsoon wind strength and associated shift in the Inter-Tropical Convergence Zone (ITCZ) influenced the dominant sediment provenance at Site U1457 of the Laxmi Basin.

1. Introduction

The Indian Summer Monsoon (ISM), one of the main components of the modern global monsoon system, plays an important role in the socio-economic scenario of the most populated tropical regions of the world (Mugnier & Huyghe, 2006). Therefore, an understanding of the origin, evolution and controls of the ISM is necessary to predict future consequences. The existence of a proto-monsoon during the Eocene has been documented from several monsoon core regions (Licht *et al.* 2014; Farnsworth *et al.* 2019) while the recorded existence of the Indian Monsoon dates back to the Miocene (~24 Ma; Clift *et al.* 2008; Zhou *et al.* 2021). Further, the environmental changes in the terrestrial ecosystem and oceanographic processes during the Miocene have been studied using a variety of geological archives to understand the Indian Monsoon system (Quade *et al.* 1989; Kroon *et al.* 1991; Quade & Cerling, 1995; An *et al.* 2001; Gupta & Thomas, 2003; Ghosh *et al.* 2004; Molnar, 2004; Clift *et al.* 2008, 2009; Betzler *et al.* 2016; Pandey *et al.* 2016; Mungekar *et al.* 2020). These geological evidences suggest that the seasonal wind reversal system was established around the late mid-Miocene (~12 Ma; Gupta *et al.* 2015; Betzler *et al.* 2016). Subsequent to the late mid-Miocene, the hydroclimatic condition in the subcontinent reflected large-scale drying which is consistent with the Miocene global cooling trend (Holbourn *et al.* 2018). The late Miocene was also a period of established monsoon seasonality and diversification of terrestrial plant and animal communities (Quade *et al.* 1989; Kroon *et al.* 1991; Prell *et al.* 1992; Quade & Cerling, 1995; Herbert *et al.* 2016). The establishment of the Indian Monsoon system is thought to be connected to the

Himalayan uplift. Although this connection remains debated, understanding of it has been greatly advanced in the past decade (Tada *et al.* 2016) through the study of marine sedimentary cores recovered during Ocean Drilling Program (ODP) expeditions. The uplift of the Himalayan–Tibetan Plateau (HTP) occurred in three phases, with uplift of the southern and central Tibetan Plateau during 40–35 Ma, of the northern Tibetan Plateau during 25–20 Ma and of the northeastern Tibetan Plateau during 15–10 Ma (Tada *et al.* 2016). The Himalayan–Tibet orogeny and subsequent establishment of the Indian Summer Monsoon system have led to the formation of Himalayan foreland basins and major submarine sedimentary sequences in the Indian Ocean, namely the Indus Fan and the Bengal Fan (Molnar & Tapponnier, 1978; Molnar, 1984; Molnar *et al.* 2010). Studies of sedimentation pattern, erosional history, sediment provenance and palaeoceanographic changes as recorded in the sedimentary archives of the Indus Fan and Bengal Fan have provided useful insights into the evolution of the ISM and its links with Himalayan mountain building (Amano & Taira, 1992; France-Lanord *et al.* 1993; Clift *et al.* 2002a, Clift, 2006; Lupker *et al.* 2013; Gupta *et al.* 2015; Clift & Webb, 2019). It was found that the ISM was largely controlled by orographic barrier, development of ice sheets, changes in the northern hemisphere glaciations, atmospheric CO₂ levels and shifting of the Inter-Tropical Convergence Zone (ITCZ) as a consequence of orbital forcing and solar insolation (Wang *et al.* 2005; YG Zhang *et al.* 2009; Clift *et al.* 2010; GJ Zhang *et al.* 2019; Thomson *et al.* 2021). Thus, it can be confirmed that the ISM has undergone multiple phases of evolution to attain modern-day strength (Clift *et al.* 2008, 2014; Zhisheng *et al.* 2015; Zhou *et al.* 2021).

The present study discusses the long-term precipitation proxies archived in the sedimentary bed of the NE Arabian Sea to investigate the continental erosion and hydroclimatic conditions in the Indus River Basin since the late Miocene. The aim of the study is to establish the timing and duration of hydroclimatic change in the Western Himalayan region and the corresponding Indus Fan sedimentation since the late Miocene. To achieve this, a chronologically well-constrained sedimentary stratigraphic sequence of the Indus Fan (Site U1457 of the Laxmi Basin) in the NE Arabian Sea was obtained during International Ocean Discovery Program (IODP) Expedition 355. The subsamples were subjected to sedimentological, environmental magnetic as well as major and trace element geochemical analysis to fingerprint the long-term hydroclimate variability and sediment provenance in the study area.

2. Study area

2.a. IODP 355 drill site U1457 in the Indus Fan

During IODP expedition 355, sedimentary cores were retrieved from the NE Arabian Sea at Sites U1456 and U1457. For this study, the sediment core (1100 m) collected from Site U1457 has been utilized to understand the sediment provenance and hydroclimatic condition over the Indus River Basin since the late Miocene. Site U1457 is situated in the Laxmi Basin, NE Arabian Sea, c. 490 km west of the Indian west coast and 760 km south of the Indus River mouth. Site U1457 is located at 17° 9.95' N, 67° 55.80' E and the water depth is 3534 m (Fig. 1a). The Laxmi Basin is separated from the rest of the Arabian Sea by the Laxmi Ridge (continental fragment) in the NE Arabian Sea (Pandey

et al. 1995). The sedimentary succession from IODP Site U1457 has been studied for lithological characteristics, micro-palaeontological and palaeomagnetism for establishing the stratigraphy (Pandey *et al.* 2016; Routledge *et al.* 2019). Based on the physical properties and lithological characteristics, the Site U1457 sediment core has been broadly categorized into five lithologic units (Pandey *et al.* 2016). Unit I (depth range from 0 to 74.4 m), deposited during the middle to late Pleistocene, is inferred as hemipelagic sediments deposited under turbidity currents. Unit II (depth range from 74.4 to 385.6 m) was deposited during the early Pleistocene (1.2 to 1.9 Ma). Unit II is interpreted as turbidite series, and the frequency and thickness of the turbidite bed varies downhole. Unit III (depth range from 385.6 to 834.9 m) was deposited during the Pliocene and the late Miocene. In Unit III, two major lithological groups, hemipelagic and redeposited turbidite deposits, are inferred. The hemipelagic and turbidite deposits occur in repeated cycle throughout Unit III. The Unit IV (depth range from 834 to 1062 m) sedimentation occurred during the late Miocene. The dominant lithology in Unit IV is claystone and silty claystone with minor amounts of calcarenite, calcilutite, breccia and limestone. Unit V (depth range from 1062 to 1092 m) was deposited during the Palaeocene. Unit V consists mainly of claystone, silty claystone and sandstone with volcanoclastic breccia and sandstone. Unit V is situated directly at the basaltic basement, and the sediments show the presence of smectite mineral which is the product of chemical weathering of the volcanic rocks. In this study, samples covering 700 m thickness from Site U1457 belonging to the Late Miocene (Unit I to Unit III) are studied for sedimentological, geochemical and environmental magnetic properties. The age–depth model has been developed using biostratigraphy, magnetostratigraphic and isotope (⁸⁷Sr/⁸⁶Sr) stratigraphy (Routledge *et al.* 2019). A summary of the age model and tie-points used to calculate sample age is given in Supplementary Table 1 (in the Supplementary Material available online at <https://doi.org/10.1017/S0016756822001273>). The average sample resolution of this study is ~104 ka for the Pleistocene, ~60 ka for the Pliocene and ~64 ka for the late Miocene.

The Indus River acts as a dominant carrier of detritus from the Western Himalaya through its tributaries (Sutlej, Jhelum, Ravi, Chenab and Beas) to the NE Arabian Sea. The Indus River supplies c. 250 Mt yr⁻¹ sediments to the Arabian Sea (Milliman & Syvitski, 1992). Sediments deposited in the Arabian Sea are the second largest submarine sedimentary body. The Indus Submarine Fan in the Arabian Sea covers an area of 1.1 × 10⁶ km² having a maximum width of 960 km and a length of 1500 km (Clift *et al.* 2001; Pandey *et al.* 2016; Fig. 1). The various bedrock domains that supply the sediment to the Arabian Sea through the Indus River include the Trans-Himalayas and the Greater and the Lesser Himalayas (Fig. 1b; Garzanti *et al.* 1987). The lithological heterogeneity belonging to various bedrock ages (Searle, 1996; Hodges, 2000; Clift & Webb, 2019) forms the major sediment provenance in the Indus Fan. In addition, the sediments derived from Deccan basalts of Peninsular India are also a contributor to the Indus Fan (Carter *et al.* 2020; Khim *et al.* 2020).

Currently, the Indus River Basin receives moisture from both the southwest monsoon and the winter monsoon through westerly jets (Karim & Veizer, 2002). Precipitation over the mainland is controlled by land–sea pressure gradients during summer and winter that bring the heat and moisture from the Indian Ocean (Cheng *et al.* 2012). The link between ISM variability and northern

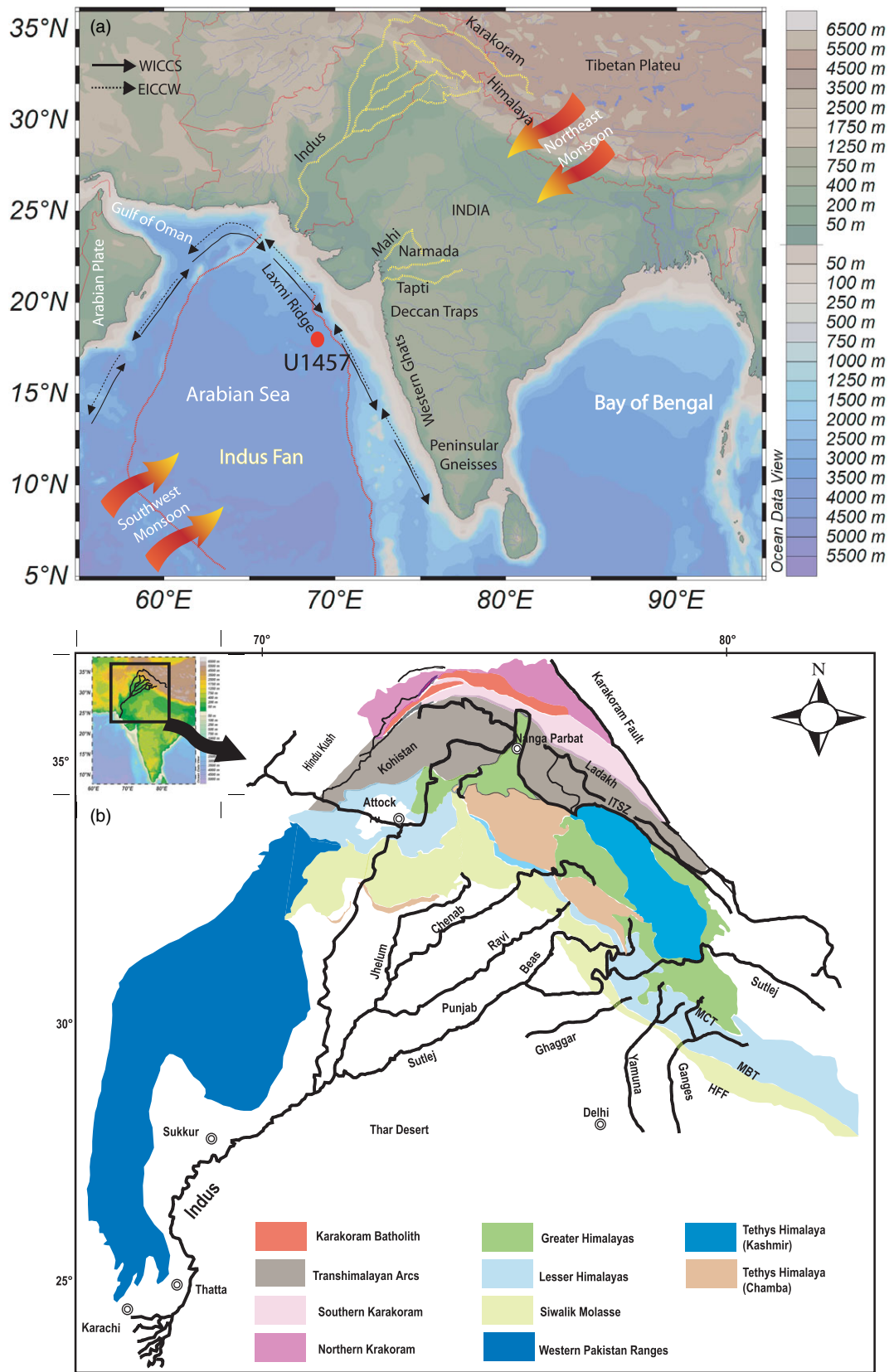


Fig. 1. (Colour online) (a) Location map of drill site U1457 in the NE Arabian Sea, and present-day drainage map of Indus River Basin draining the western Himalayas. The Indus River is the chief contributor of terrestrial sediments to the Indus Fan in the eastern Arabian Sea through its main distributor channels draining the Himalayan and Tibetan Plateau. Schematic representation of wind direction during SW monsoon and NE monsoon seasons is given. WICCS indicates the West Indian Coastal Current in summer and EICCW represents the East Indian Coastal Current in winter. (b) Geological map of Indus River Basin draining western Himalayas. Abbreviations: MCT – Main Central Thrust; MBT – Main Boundary Thrust; HFF – Himadri Frontal Fault; ITSZ – Indus–Tsangpo suture zone.

hemisphere summer insolation is also established on an orbital timescale which occurs in conjunction with the cross-equatorial latent heat transport from the southern Indian Ocean (Clemens *et al.* 1991; Clemens & Prell, 2003). The summer monsoon controls the humidity and temperature over the continents, which in turn govern the intensity of chemical weathering and erosion in the source region (Tada *et al.* 2016).

2.b. Surface hydrography and oceanography of the northeastern Arabian Sea

The northern Indian Ocean experiences changes in surface hydrography primarily due to variations in monsoonal wind patterns (Banse, 1987; Brock *et al.* 1994; Luis & Kawamura, 2004). The clockwise West Indian Coastal Current (WICC) carries high-salinity water from the northern Arabian Sea to the south (Schott, 1983; Shetye *et al.* 1991; Kumar *et al.* 2004) during the summer monsoon season (June–September). As the wind system reverses, the East Indian Coastal Current (EICW) carrying low-salinity water from the northern Bay of Bengal replenishes the SE Arabian Sea, leaving the WICC to flow to the north along the west coast of India (November–February; Shetye *et al.* 1991; Kumar *et al.* 2004).

3. Methodology

The sediment cores were subsampled at *c.* 1.5 m intervals (one sample per section). The sediment subsamples ($n = 330$) were air-dried until complete dryness. For grain-size analysis, an aliquot (1 g) of sediment samples ($n = 270$) was treated with hydrochloric acid (HCl; 10 %) to remove the carbonates, and then with hydrogen peroxide (H_2O_2 ; 30 %) to remove organic matter. The sediment sample was separated through centrifugation after each sample treatment step. Further, the samples were dispersed by adding sodium hexametaphosphate solution (1 %). Grain-size analysis was performed using the Beckman Coulter® Laser Diffraction Particle Size analyser, and sedimentary parameters were determined using the Gradistat® excel spreadsheet (Blott & Pye, 2001). The acid-resistant fraction (ARF) of sediment was estimated gravimetrically after the removal of organic and dissolved inorganic fractions of sediment by chemical treatment with H_2O_2 and HCl. The repeated centrifugation and decantation of the solution led to an acceptable limit (<10 %) of material loss.

Lithogenous mass accumulation rate (LMAR) is estimated using the following equation provided by Davies *et al.* (1995):

$$LMAR = LSR(\text{cm ka}^{-1}) \times ARF(\%) \times DBD(\text{g cm}^{-3})$$

where LSR is linear sedimentation rate, ARF is acid-resistant fraction of sediment and DBD is average dry bulk density (data taken from Pandey *et al.* 2016).

For geochemical measurement of major and trace elements, *c.* 100 mg of dried and finely powdered sediment samples were acid-digested using the microwave digestion system (Speed Wave MWS-3, Analytical Jena, Germany). The sediment samples were decomposed using two steps of acid digestion. The first step includes addition of nitric acid (HNO_3 , 60 %) and hydrogen peroxide (H_2O_2 , 30 %) with stepwise heating up to 220 °C. Hydrofluoric acid (HF; 46 %) was added along with nitric acid (HNO_3 , 60 %) and hydrogen peroxide (H_2O_2 , 30 %) mixture and again heated up to 220 °C in the microwave digestion system. The clear solutions were transferred to Perfluoroalkoxy alkanes (PFA) vials (Savilleux, USA) and evaporated to complete dryness. The insoluble fluoride

precipitates were removed using hydrochloric acid (HCl, 36 %). Completely digested sample residues were dissolved in 5 % HNO_3 for major and trace element analysis. The major and trace element measurements were carried out using inductively coupled plasma – optical emission spectrometry (ICP-OES) and ICP – mass spectrometry (ICP-MS) respectively using the calibration curve method. The background concentration is corrected using simultaneous measurements of blank and standard (standard bracketing method). The relative standard deviation (r.s.d.) of replicate measurements was within ± 3 %. The accuracy of measurements was cross-checked using geochemical reference materials JMS-1 and JMS-2, and was found to be within acceptable limits.

The chemical index of alteration (CIA) was calculated using the following equations (Nesbitt & Markovics, 1980; Nesbitt & Young, 1984). The CIA was further modified to CIA* corrected for carbonates (Fedó *et al.* 1995; Singh *et al.* 2005; Tripathy *et al.* 2014).

$$CIA = (Al_2O_3/Al_2O_3 + Na_2O + K_2O + CaO^*) \times 100$$

$$CIA^* = (Al_2O_3/Al_2O_3 + Na_2O + K_2O) \times 100$$

All the major oxides used in the calculation were a molecular proportion of the silicate fraction, and CaO^* is the amount of CaO incorporated into the silicate fraction.

The terrigenous magnetic minerals (e.g. iron-bearing oxides and hydroxides) deposited in the form of marine sediments carry information that can be used to reconstruct palaeoclimate, palaeoproductivity and palaeoenvironmental changes (Evans & Heller, 2003). For various environmental magnetic mineral measurements, the sediment samples (3–4 g) were tightly packed in a standard 8 cc cylindrical plastic bottle. The prepared samples were subjected to environmental magnetic measurements like magnetic susceptibility (χ_{lf}), anhysteretic remanent magnetization (ARM), saturation isothermal remanent magnetization (SIRM) and its DC demagnetization (Walden, 1999). Low-frequency magnetic susceptibility (χ_{lf}) measurement was carried out with a Bartington magnetic susceptibility meter (model MS2B) operating at a frequency of 0.47 kHz and field intensity of 200 Am^{-1} . The ARM was imparted by exposing the samples to an alternating linearly decaying magnetic field of 100 mT peak field in the presence of a DC bias field of 0.05 mT using a D-2000T alternating field demagnetizer (ASC Scientific, USA). The ARM intensity was measured using the dual-speed JR-6 spinner magnetometer (AGICO, Czech Republic). The ARM is usually expressed as the susceptibility of ARM, i.e. $\chi_{ARM} (\text{m}^3 \text{kg}^{-1}) = ARM/39.79$ (where 39.79 represents the size of the biasing field at 0.05 mT = 39.79 $A \text{ m}^{-1}$). SIRM was induced in a 1 Tesla steady pulse-field using an ASC Scientific IM-10-30 model impulse magnetizer. After SIRM acquisition, backfields of 20, 30, 100 and 300 mT were applied. The soft IRM (SIRM-IRM@-30mT) and hard IRM (SIRM-IRM@-300mT) were then calculated to determine the soft ferrimagnetic magnetite and hard antiferromagnetic haematite respectively. The S-ratio which quantifies the relative proportion of soft and hard magnetic minerals within the sediment sample (Stober & Thompson, 1979; King & Channell, 1991; Stoner *et al.* 1996) was calculated using the expression, S-ratio = $IRM_{@-300mT}/SIRM$. In general, the S-ratio ≈ 1 indicates a relative abundance of magnetite compared to haematite while the S-ratio < 0.9 indicates a relative abundance of haematite over magnetite in the analysed sample. The magnitudes of measured magnetic parameters were independently sensitive to the concentration of ferrimagnetic and anti-ferromagnetic minerals whereas the calculated interparametric ratio (χ_{ARM}/χ_{lf}) was

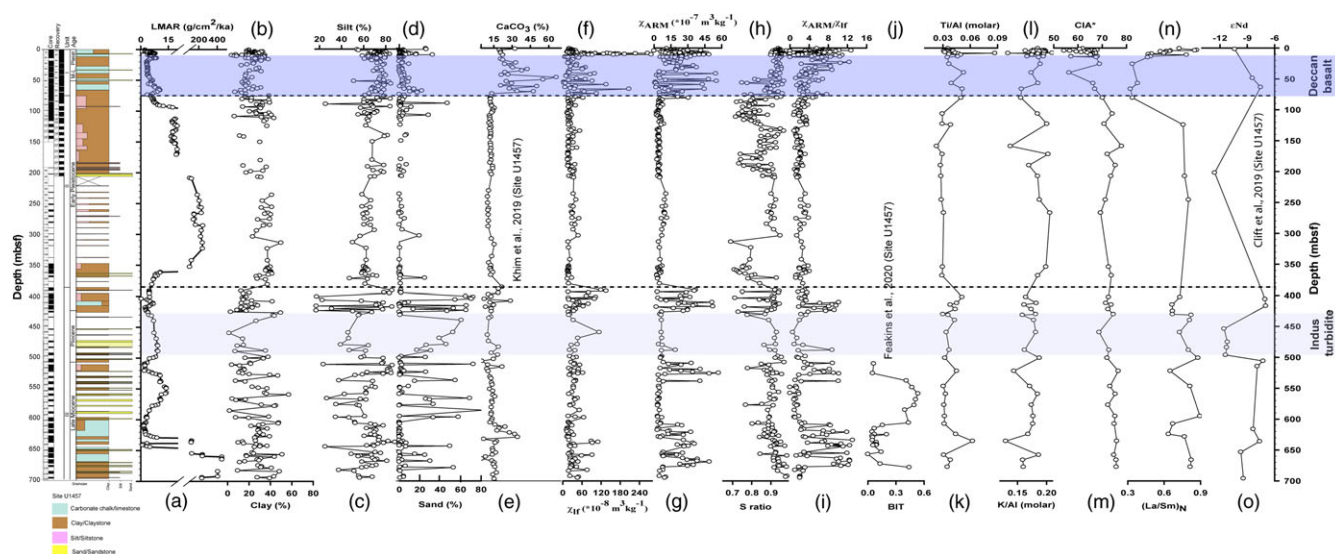


Fig. 2. (Colour online) The sedimentological, environmental magnetic and geochemical proxies plotted against the lithostratigraphy of Site U1457. (a) Lithogenous mass accumulation rate (LMAR), percentage of sediment grain-size parameter: (b) clay, (c) silt, (d) sand, (e) calcium carbonate (CaCO_3 ; Khim *et al.* 2020b), (f) χ_{16} , (g) χ_{ARM} , (h) S-ratio, (i) χ_{ARM}/χ_{16} , (j) branched and isoprenoid tetraether (BIT; Feakins *et al.* 2020), (k) Ti/Al molar, (l) K/Al molar, (m) Chemical Index of Alteration (CIA^*), (n) $(\text{La}/\text{Sm})_N$ and (o) ϵ_{Nd} (Clift *et al.* 2019) at Site U1457.

indicative of magnetic grain size (Thompson & Oldfield, 1986; Maher, 1988; Oldfield, 1991).

4. Results

The results of the sedimentological, environmental magnetic, and geochemical dataset for the IODP drill Site U1457 of the Arabian Sea are given in Supplementary Tables 2 and 3 (in the Supplementary Material available online at <https://doi.org/10.1017/S0016756822001273>). The depth-wise variation (Fig. 2) and temporal variation in lithological, textural, magnetic and geochemical proxies are represented graphically (Figs 3 and 4) to infer the obtained results. The estimated linear mass accumulation rate (LMAR) in the drill site varied from $0.1 \text{ g cm}^{-2} \text{ ka}^{-1}$ to $574 \text{ g cm}^{-2} \text{ ka}^{-1}$ (avg. $19.2 \text{ g cm}^{-2} \text{ ka}^{-1}$). The maximum sedimentation rate was observed at 7.5 Ma (max. $574 \text{ g cm}^{-2} \text{ ka}^{-1}$), from 6.1 Ma to 5.6 Ma (avg. $11 \text{ g cm}^{-2} \text{ ka}^{-1}$) and from 1.7 Ma to 0.02 Ma (avg. $21 \text{ g cm}^{-2} \text{ ka}^{-1}$; Fig. 3). The sediment mean grain size (MGS) was in the range $3.11 \mu\text{m}$ to $154 \mu\text{m}$ (avg. $8.03 \mu\text{m}$; data point of $154 \mu\text{m}$ is not shown in the figure). The MGS showed an overall decrease during the late Miocene, except for the period 6.1 Ma to 5.6 Ma during which the MGS was higher. The MGS increased during the Pliocene and the Pleistocene; however, prominent variability was observed during the Pleistocene. The ARF at the drill site varied from 12 % to 97 % (avg. 47 %) of the sediment weight. The ARF was relatively higher during the Pleistocene.

The sediment texture in the core was dominated by silty-clay fraction (Fig. 2). The silt fraction varied from 12 to 100 % (avg. 65 %) while the clay fraction varied from 2 to 57 % (avg. 26 %) and sand fraction varied from 0 to 82 % (avg. 8 %). The silt clay fraction of sediment showed long-term increase during the late Miocene, except for the period 6.1 Ma to 5.6 Ma during which the silt clay fraction was lower. During the Pliocene, the silt clay fraction of sediment increased from 4 Ma to 3.6 Ma, after which it showed a declining trend till 2.5 Ma. During the Pleistocene, the silt clay fraction showed general uniform depth distribution, with silt being the dominant grain fraction. The sediment sorting

(ϕ) varied from 0.35 to 3.19 (avg. 1.56), skewness (ψ) varied from -0.34 to 0.56 (avg. 0.17), and the Kurtosis (θ) varied from 0.62 to 2.56 (avg. 1.12) at Site U1457. The sorting and skewness indicated poorly to very poorly sorted sediment, possibly due to involvement of different transport agencies.

The index of clastic sediment flux, Ti/Al, showed an overall increase since the late Miocene, with significant decrease during the late Pleistocene (1.6–1.2 Ma) and the Miocene (5.9–5.5 Ma). The silicate weathering proxy, K/Al, varied from 0.13 to 0.21 (avg. 0.18). The K/Al ratio during the late Miocene showed an increase, except for the period 7.5 Ma to 7 Ma during which the K/Al ratio decreased. The K/Al ratio in the Pliocene increased, while it decreased with an observable cyclicity during the Pleistocene (Fig. 3). The chemical index of alteration (CIA) varied from 56 to 76 in the sediment core, with an overall decrease since the late Miocene. The Mg/Al varied from 0.25 to 0.86 (avg. 0.52), Fe/Al varied from 0.17 to 0.44 (avg. 0.30), Co/Al varied from 5.33 to 50.07 (avg. 15.46) and Cr/Al varied from 15.02 to 36.47 (avg. 23.73). The Mg/Al, Fe/Al, Co/Al and Cr/Al showed similar variability, with higher values during the late Miocene (except for the time period from 5.9 to 5.5 Ma) and the Pliocene, and lower values during the Pleistocene (1.9 to 1.2 Ma) and the late Miocene (5.9 to 5.5). Upper continental crust (Taylor & McLennan, 1985) normalized $(\text{La}/\text{Sm})_N$ varied from 0.29 to 1.34 (avg. 0.74). The $(\text{La}/\text{Sm})_N$ values remained low during the late Miocene. However, slightly higher values were observed at 5.9 to 5.5 Ma and 7 Ma. Consistently higher values of $(\text{La}/\text{Sm})_N$ were observed during the Pliocene, while $(\text{La}/\text{Sm})_N$ values declined during the late Pleistocene. Low $(\text{La}/\text{Sm})_N$ values were observed during 1.2 to 0.42 Ma, after which the values showed an increase. The concentrations of major and trace elements in the sediment core did not show a statistically significant correlation with sediment mean grain size.

χ_{16} , χ_{ARM} and SIRM varied in the range 3 to 277 (avg. 40), 0.8 to 74 (avg. 16) and 3 to 406 (avg. 56) respectively in the sediment core at Site U1457. The calculated S-ratio varied from 0.5 to 1.0 with an average value of 0.9 in the studied core. The soft IRM and hard IRM

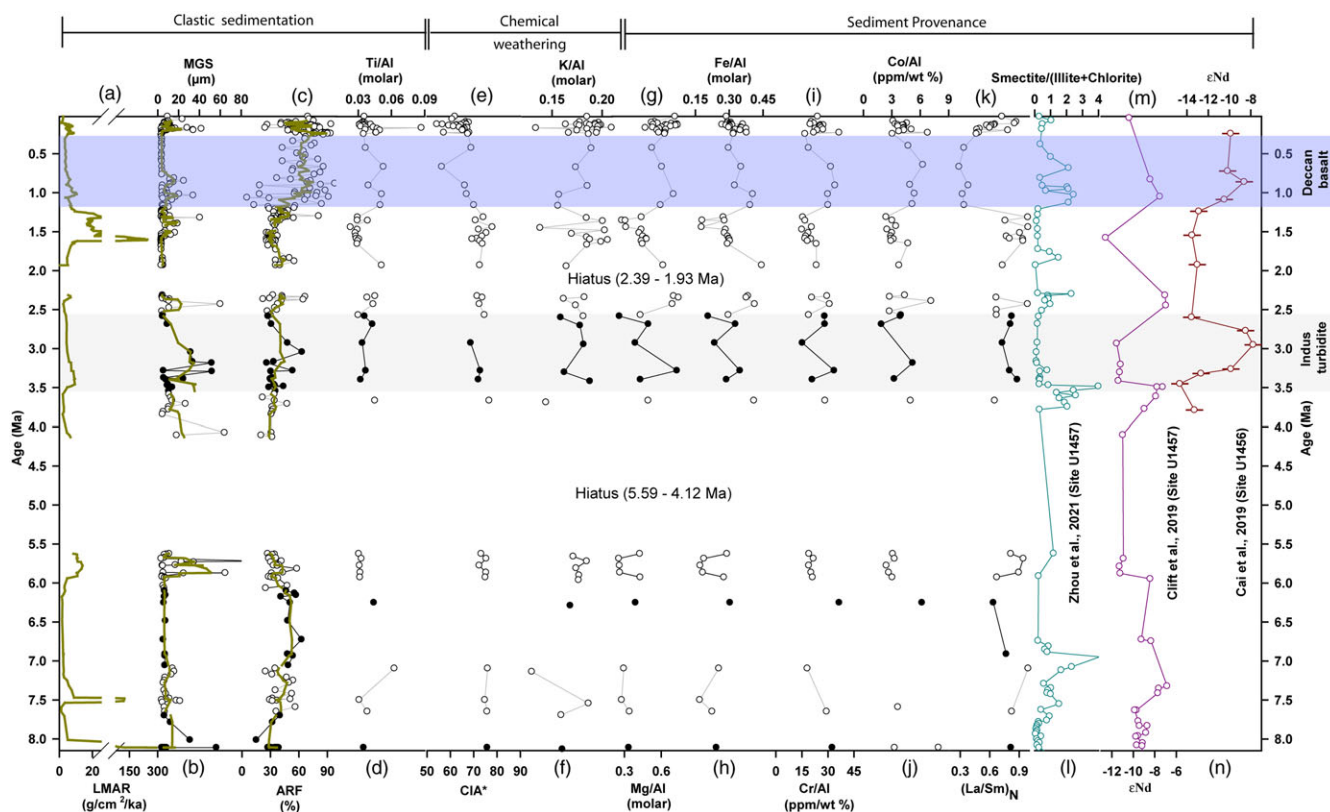


Fig. 3. (Colour online) (a) Lithogenous mass accumulation rate (LMAR), (b) mean grain size (MGS), (c) acid-resistant fraction (ARF), (d) Ti/Al, (e) Chemical Index of Alteration (CIA*), (f) silicate weathering index, K/Al (molar), (g) Mg/Al (molar), (h) Fe/Al (molar), (i) Cr/Al (ppm/wt %), (j) Co/Al (ppm/wt %), (k) (La/Sm)_N, (l) smectite/illite+chlorite (Zhou *et al.* 2021) and (m, n) ϵ_{Nd} from drill sites U1457 (Clift *et al.* 2019) and U1456 (Cai *et al.* 2019), NE Arabian Sea, and comparison with the isotopic composition (ϵ_{Nd}) of clastic sediments from the same drill site U1457. In (a–c), a five-point moving average of respective data series is plotted in solid dark-green lines; solid black circle indicates the dry condition while empty circle shows the humid condition in the NE Arabian Sea.

varied from 2 to 293 (avg. 43) and 4 to 614 (avg. 46) respectively, while the interparametric ratio (χ_{ARM}/χ_{lf}) varied from 0.6 to 13 (avg. 4). The environmental magnetic parameters (χ_{lf} , χ_{ARM} and SIRM) showed synchronous variation through time in the NE Arabian Sea. Synchronous variability was also observed among S-ratio, soft IRM and hard IRM (Fig. 4). A consistent long-term trend of synchronous variability was also observed between the interparametric ratios (χ_{ARM}/χ_{lf} and $\chi_{ARM}/SIRM$) and χ_{ARM} . Therefore, the single interparametric ratio (χ_{ARM}/χ_{lf}) was used to explain magnetic grain size. In general, the data pattern showed an increase in magnetic mineral concentration (χ_{lf}) and ferromagnetic minerals (χ_{ARM}) from the late Miocene to the late Quaternary. The magnetic mineral concentration, magnetic mineral grain size and magnetic mineralogy showed significant variability since the late Miocene (Fig. 4). Based on the magnetic concentration, magnetic grain size and magnetic mineralogy, shifts in sediment erosion and sedimentation pattern were identified, at 7.5 Ma to 7 Ma, 6 Ma to 5.6 Ma, 3.6 Ma to 2.4 Ma, 1.7 Ma to 1.2 Ma, and 1.2 Ma to Recent time (Fig. 4). There was a good correlation ($R^2 = 0.735$) between χ_{lf} and SIRM in the studied sedimentary sequence. The correlation among environmental magnetic parameters and sedimentary mean grain size was poor at study site U1457.

The IRM acquisition curves of samples ($n = 16$) saturated at higher field of >500 mT (Fig. 5a). The progressive removal of SIRM by applying reverse fields indicated that the remanent coercivity (H_{cr}) varied between *c.* 25 and 75 mT (inset of Fig. 5a), suggesting that

both low-coercivity magnetite and high-coercivity haematite magnetic mineral phases existed (Dunlo & Özdemir, 1997). On the other hand, the IRM acquisition curves of some sediment samples reached saturation at >750 mT (Fig. 5b). These samples may contain high-coercivity haematite with very high H_{cr} values (45 and 100 mT; inset of Fig. 5b).

The magnetic mineral carriers have been determined by temperature dependence of magnetic susceptibility (χ -T) measurements in selected samples of the sediment core. The representative χ -T curves are shown in Figure 5c–f. Samples with magnetic mineral carriers dominated by Curie temperatures (T_c) at ~ 580 °C and 685 °C suggested the presence of both magnetite and haematite as the dominant magnetic mineral carriers (Fig. 5c–f). However, some sediment samples did not have clear Curie temperature transitions at 580 °C or 685 °C, suggesting that the data was too noisy and cannot be interpreted (Fig. 5d–e).

5. Discussion

The dataset generated from this study on Site U1457 (Supplementary Table 2 in the Supplementary Material available online at <https://doi.org/10.1017/S0016756822001273>) has been discussed in conjunction with the published neodymium isotopic dataset (ϵ_{Nd} ; Clift *et al.* 2019b; Zhou *et al.* 2021), CaCO₃, TOC (Khim *et al.* 2020b) and branched and isoprenoid tetra-ether (BIT) datasets (Feakins *et al.* 2020) (i) to check for possible influence of *in situ* authigenic processes on the proxy signatures, (ii) to

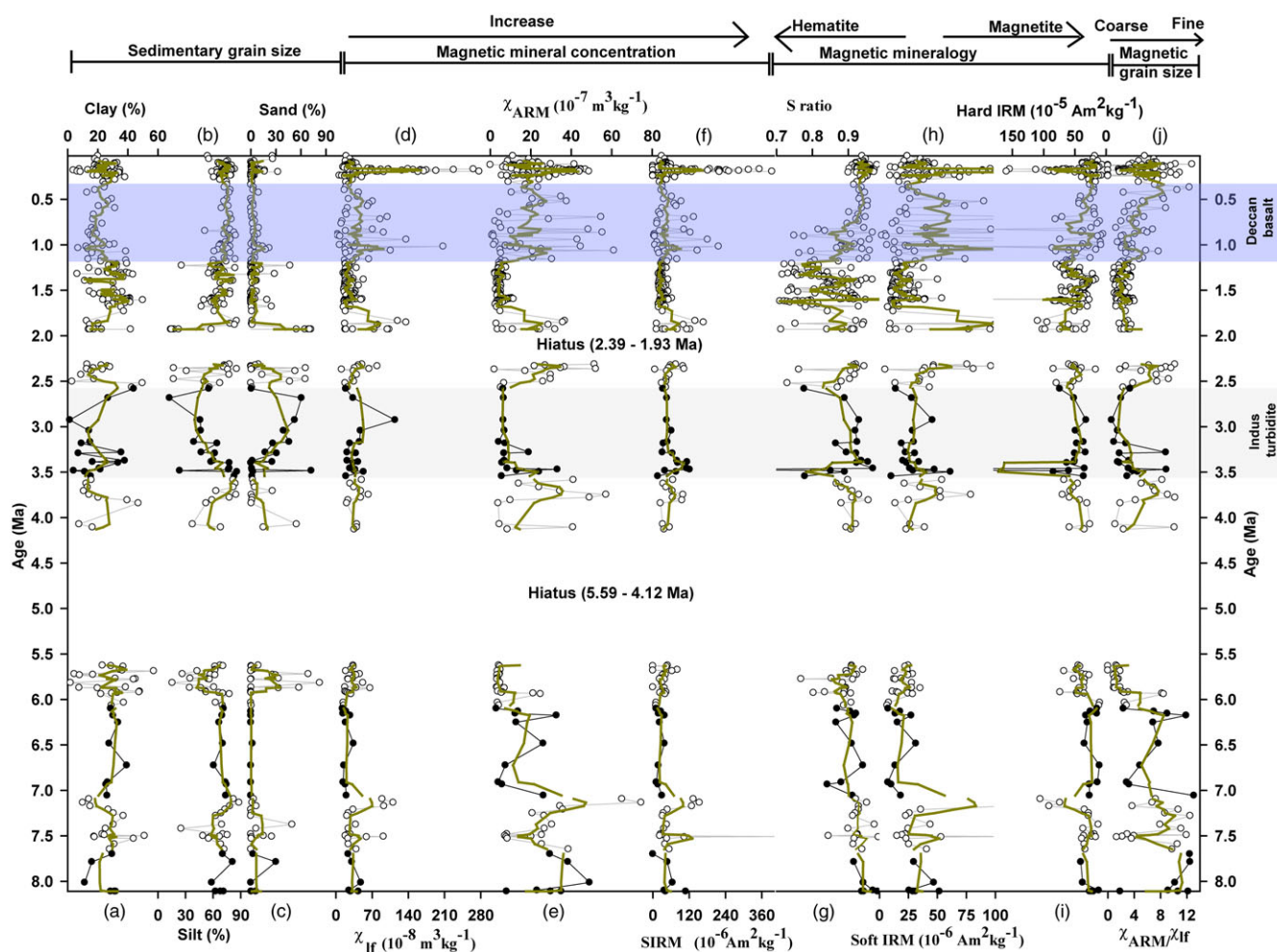


Fig. 4. (Colour online) Sedimentary grain size (a–c) indicates clay, silt and sand in %. Magnetic mineral concentration: (d) χ_{If} , (e) χ_{ARM} and (f) SIRM; magnetic mineralogy: (g) S-ratio, (h) soft IRM and (i) hard IRM. (j) χ_{ARM}/χ_{If} , interparametric ratio of magnetic data for Indus River Basin record from the eastern Arabian Sea drill site U1457.

determine the sediment provenance in the Indus Fan and (iii) to understand the erosional history of the Indus River Basin and Peninsular India, and its link with summer monsoon which further provides insight into the climate variability over the Indian subcontinent since the late Miocene.

5.a. Depth profile of proxy signatures and their variation with respect to lithostratigraphy

The reliability of proxy for the interpretation of terrestrial processes must be carefully considered as sediments deposited under the influence of turbidity current and autocyclic processes within basin affect the sedimentation rate, sediment sorting and the geochemical proxy signatures. Earlier workers have provided lithostratigraphic framework and inferred the depositional conditions for Site U1457 (Pandey *et al.* 2016; Routledge *et al.* 2019; Feakins *et al.* 2020). In this study, the depth profiles of proxy signatures along with lithostratigraphy are plotted to differentiate redeposited turbidite deposits (autocyclic process within the basin) and hemipelagic sediments as they have implications on terrestrial hydroclimate and within-basin depositional processes (Fig. 5). The sediment grain size in Unit I is dominated by clay and silt with high percentage of biogenic CaCO_3 suggesting hemipelagic sedimentation. Unit II is composed of massive deposits of silty

clay interbedded with very thin, grey sandy silt layers. The sandy layers occur in a cyclic manner throughout Unit II. Based on dominance of silt and clay with a consistently low percentage of biogenic carbonates, Unit II is interpreted as turbidite series, and the frequency and thickness of the turbidite bed varies. However, the sediment deposited in Unit II is considered as a product of the sedimentation in a basin plain environment (Pandey *et al.* 2016). In Unit III, two major lithological groups, hemipelagic and redeposited turbidite deposits, were distinguished. The hemipelagic and turbidite deposits occur in repeated cycle throughout Unit III. The fine-grained and partly biogenic sediments between 385 and 440 m are inferred to be deposited in a basin plain setting or on the edge of an active lobe. Alternating sandy turbidity deposits, below 440 m depth, are deposited in the active lobe environments separated by hemipelagic sediments at depths of 540–500 m and 600–670 m (Pandey *et al.* 2016; Feakins *et al.* 2020). The grain-size data from this study suggests that Unit III is composed of silt and clay with sand fraction (maximum up to 65 %). The sand fraction in Unit III fluctuates, except for the depth from 440 m to 500 m where there is a continuous increase in sand content. Based on sediment grain size and sedimentation rate, the hydrodynamic depositional conditions for these sand deposits were inferred: (i) redeposited turbidite sediments (depth from 440 m to 500 m), and (ii) sandy

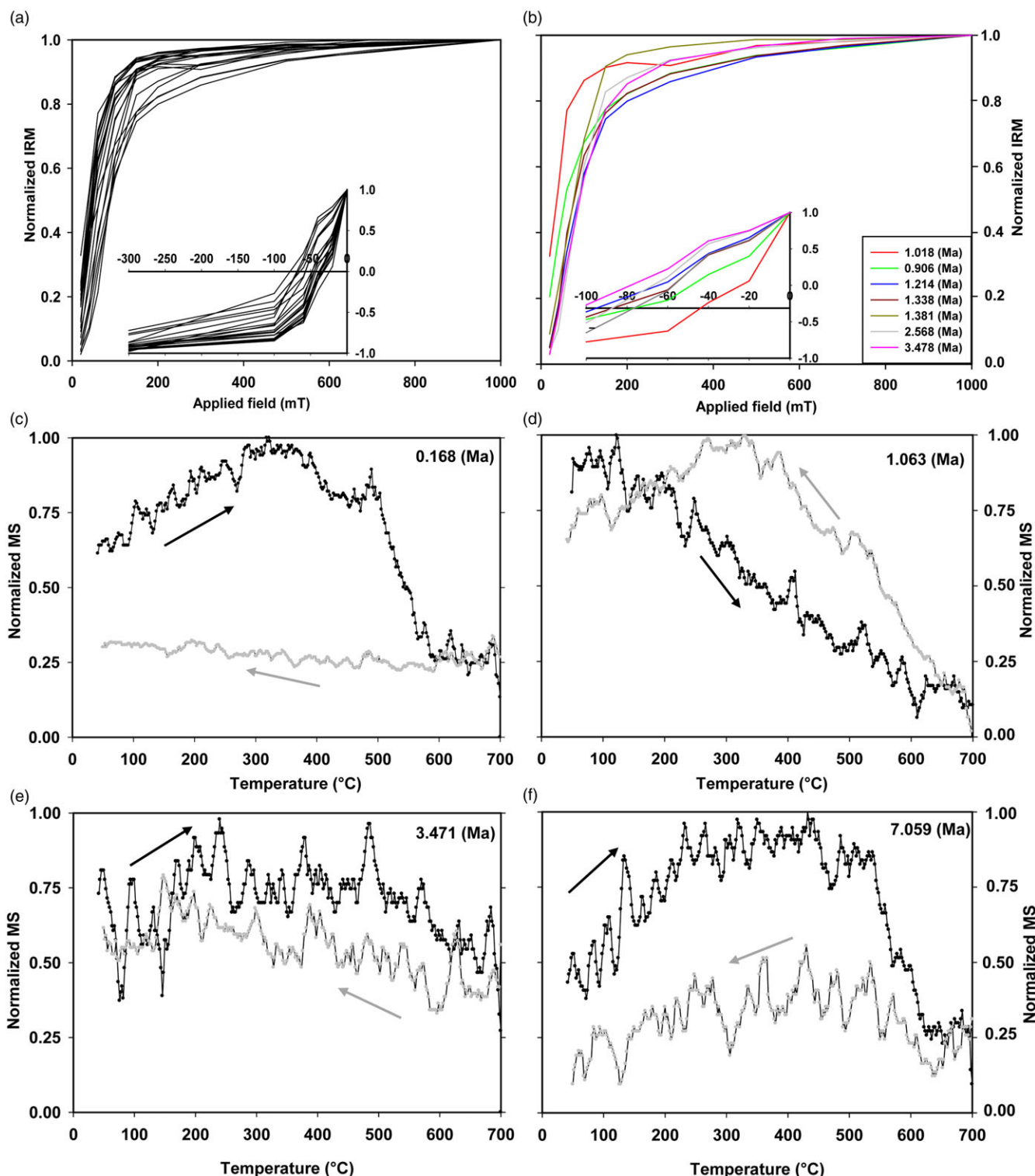


Fig. 5. (Colour online) IRM acquisition curves for representative sediment samples to identify magnetite and haematite magnetic minerals. The normalized IRM vs applied field (mT) plots (a, b) discriminate the dominant presence of haematite and magnetite minerals in the samples. The χ -T curves indicate presence of both magnetite and haematite during the late Miocene and Pleistocene (c, f). (d, e) show the noise level and the difficult-to-differentiate magnetic mineralogy. The black and grey curves and arrows represent heating and cooling respectively.

sediment deposited under high-energy conditions (depth from 500 m to 600 m).

The sandy sediments can be deposited under different hydrodynamic conditions such as (i) high river discharge from the continents, (ii) storm activity within the oceans and (iii) turbidite

current deposits, or a combination of all three conditions. The sand-dominated sediment deposits in the depth range from 440 m to 500 m (age 3.5–2.5 Ma) exhibit continuous increase in sand content, low CaCO_3 , and coarse-grained magnetic minerals. Further, the ϵ_{Nd} values of these deposits at Site U1457 are more

negative than those of sediments deposited at Site U1456. Such heterogeneity in ϵ_{Nd} among the drill sites could arise from the changes in sediment source. The Indus River sediment provenance in Site U1457 and Deccan-basalt-derived sediment provenance in Site U1456 (Cai *et al.* 2019) could be due to autocyclic process within the basin at 440 m to 500 m (age 3.5–2.5 Ma). Therefore, the proxy signatures of sediment deposits in the depth range from 440 m to 500 m (age 3.5–2.5 Ma) could be a reflection of the depositional processes within the basin rather than terrestrial hydroclimatic conditions of the Indus Basin. On the other hand, the sediment deposits in the depth range from 540 m to 600 m (age 6.0–5.6 Ma) are interpreted as turbidites (Pandey *et al.* 2016; Feakins *et al.* 2020), and alternating clay–silt dominated sediments as hemiplegic sediments. The fluctuating sand fraction of the sediments, low biogenic carbonates, terrestrial organic matter and Indus River provenance (ϵ_{Nd}) in sediments suggest that the sedimentation occurred in the Indus river mouth or more likely the distal portion of the fan. Therefore, the proxy signatures from Site U1457 probably reflect the terrestrial hydroclimatic conditions and sedimentary provenance in the source area, except for the late Pliocene time interval (3.5–2.5 Ma).

5.b. Suitability of magnetic mineral proxy signatures for palaeo-monsoon reconstruction at Site U1457

The mineral magnetic parameters are sensitive to reductive diagenetic processes in the sediments (Thompson & Oldfield, 1986; Maher & Thompson, 1992; Verosub & Roberts, 1995; Evans & Heller, 2003; Liu *et al.* 2004; Reilly *et al.* 2020). The chemical environments (oxic to methanic) and related respiration (aerobic to methanogenesis) processes are well defined in the early diagenetic sediments (Canfield & Thamdrup, 2009). The magnetic minerals undergo alteration due to the reductive dissolution of Fe-oxyhydroxides, and subsequent formation of Fe-sulphides (pyrites and greigite) in the sulphidic environments due to reaction between dissolved Fe and H_2S in the marine sediments (Roberts, 2015). In ferruginous environments, the dissolved iron concentration increases in the pore water and the dissolved iron diffuses upward from pore water to the surface sediments to form oxidized iron phases (magnetite, haematite, oxyhydroxide, ferrihydrite; Berner, 1981). Under the oxic–anoxic boundary condition, the magnetotactic bacteria produce authigenic magnetite. This bacteria-mediated authigenic magnetite in sediments exhibits interparametric ratios χ_{ARM}/χ_{IF} greater than 40 and $\chi_{ARM}/SIRM$ greater than 1000 (Dearing, 1999; Walden *et al.* 1999). Thus, the development of chemical environments and the associated respiration process in sediments alter the source magnetic mineral characteristics. Therefore, it is imperative to assess the effect of diagenetic process on the mineral magnetic proxy signatures in marine sediments before deriving the palaeoenvironmental inferences.

At Site U1457, the interparametric ratios of χ_{ARM}/χ_{IF} and $\chi_{ARM}/SIRM$ in analysed sediments were less than the threshold values (<40 and <1000 respectively), indicating negligible role of magnetotactic bacterial activity in the sediments (Dearing, 1999; Walden *et al.* 1999). In addition, the magnetic mineral concentration varied positively with detritus content (ARF) at Site U1457, indicating strong source control rather than sedimentary reductive diagenesis. The magnetic versus sedimentary grain-size diagram shows that higher magnetic concentration is associated with lower clay content, which implies that the environmental magnetic signature is primarily controlled by the sediment provenance with minor sedimentary grain-size control at Site U1457

(Supplementary Fig. S1 in the Supplementary Material available online at <https://doi.org/10.1017/S0016756822001273>).

The minimal diagenetic impact on the magnetic parameters of sediments at Site U1457 can be further elucidated with the existing knowledge database on the study site. The magnetic mineral concentration is expected to be low and the magnetic grain size to be coarser in sediments deposited under reductive diagenetic sediment (Dillon & Bleil, 2006; Roberts, 2015). On the other hand, fining of magnetic grain size is expected under strong diagenetic dissolution under sulphidic conditions due to addition of authigenic minerals under euxinic conditions (Garming *et al.* 2005). At Site U1457 of the NE Arabian Sea, the depositional environment was mostly oxic and oxic–suboxic since the late Miocene (Alam *et al.* 2022). Though the suboxic depositional conditions were observed for the mid-Pliocene (3.1 Ma to 2.8 Ma) and late Pleistocene (<1.2 Ma), the depositional conditions at Site U1457 were never sulphidic since the late Miocene (Alam *et al.* 2022). Both the reduced oxygen time periods (1.75–1.12 Ma and 3.56–2.58 Ma) and oxic time interval (6.06–5.62 Ma) of Site U1457 reflected similar magnetic signatures (low magnetic concentrations (χ_{IF} , χ_{ARM} and SIRM) and coarser magnetic grain size) and organic preservation less than 1 % (Khim *et al.* 2020b). The mineralogy was dominated by high-coercivity magnetic minerals (haematite; S-ratio < 0.9) and lower bacterial magnetite activity (χ_{ARM}/χ_{IF} and $\chi_{ARM}/SIRM$ values below the threshold value; Dearing, 1999; Walden *et al.* 1999). Further, the interstitial water chemistry suggested that the sulphate reduction zone was located up to 54 meters below sea floor (mbsf) of Site U1457 sediments (Pandey *et al.* 2016; Carter *et al.* 2017). These findings confirm that the magnetic mineral signatures are largely controlled by the change in magnetic mineral provenance rather than reductive diagenesis for the study period at Site U1457. Moreover, the LMARs, sediment texture and geochemical parameter at Site U1457 showed temporal variation coinciding with global climatic events as well as provenance change in the Indus Fan. Thus, the measured magnetic proxies in this study are useful in exploring the long-term sediment sources to Site U1457 of the Laxmi Basin, and the connection of Indian subcontinental erosion and monsoonal climate evolution since the late Miocene.

5.c. Provenance of sediments at Site U1457 of the Laxmi Basin

The environmental magnetic and geochemical characteristics of sediments have been used to infer the Indus Fan sediment provenance since the late Miocene. The rationale for using environmental magnetism for provenance tracing includes (i) the major source of Indus Fan sedimentation is through the Indus River with a minor contribution from primitive igneous rocks derived from Deccan Province / Trans-Himalayas, and (ii) the magnetic mineral concentration of primitive igneous rocks (mafic rocks) is higher than that of felsic rocks, owing to differences in abundance of ferri-magnetic and diamagnetic minerals (Clark & Emerson, 1991; Sebastian *et al.* 2019). Therefore, the erosional products of mafic and felsic rocks carry differing magnetic mineral concentrations and mineralogy. An understanding of sediment provenance is a prerequisite for robust inferences on hydroclimatic and palaeoenvironmental conditions in the catchment area. This is because the heterogeneity in lithological compositions and their contrasting response to hydroclimatic changes lead to misleading palaeoclimatic inferences (Weltje & von Eynatten, 2004).

Earlier studies on the sediment provenance at IODP drill Sites U1456 and U1457 have revealed that the Indus River is the primary

contributor of sediments to the drill sites (Clift *et al.* 2019; Khim *et al.* 2020b). Further, the isotopic ($^{87}\text{Sr}/^{86}\text{Sr}$ and ϵ_{Nd}) tracing of Indus Fan sediment provenance revealed a shift in regional catchment erosion from Karakoram during the late Miocene (~9.5 Ma) to the Himalayas owing to its basin tectonics and monsoon strength (Clift & Blusztajn, 2005; Clift *et al.* 2019). However, an additional source of primitive igneous rock-derived sediments from either Deccan basalts or the Trans-Himalayan region was observed at the drill sites (Cai *et al.* 2019; Chen *et al.* 2019; Khim *et al.* 2020a). The clay mineralogy (smectite / chlorite + illite ratio), magnetic susceptibility and isotopic ($^{87}\text{Sr}/^{86}\text{Sr}$ and ϵ_{Nd}) studies on IODP drill sites U1456 and U1457 have pinpointed the source of primitive igneous rock sediments to Deccan Province, particularly during the Pliocene (3.5 Ma) and the Pleistocene (1.2 Ma to Recent; Cai *et al.* 2019; Chen *et al.* 2019; Yu *et al.* 2019; Khim *et al.* 2020a). Further, the contribution of sediments from the Deccan basalt to IODP 355 site U1456 in the NE Arabian Sea have increased during the Pliocene (3.5 Ma) and the Pleistocene (1.2 Ma to Recent; Cai *et al.* 2019; Yu *et al.* 2019; Carter *et al.* 2020) as a consequence of the weakened ISM and southward migration of the ITCZ (Carter *et al.* 2020).

In this study, the A–CN–K (Al_2O_3 –($\text{CaO}^* + \text{Na}_2\text{O}$)– K_2O) ternary diagram has been plotted to infer the weathering pattern and possible sediment source at Site U1457 (Fig. 6). The plot suggests that the major and trace elements were supplied by clastic sediments derived from the Indus River and the Peninsular Indian Rivers at Site U1457. The relative enrichment of Al and depletion of Ca, K and Na in the sediments of Site U1457 indicated the relative intensity of weathering in the source catchment area. The CIA* values (varying between 54 and 78) suggested low to moderate chemical weathering of source rocks. In the A–CN–K plot, the majority of the samples were plotted along the weathering trend line parallel to the A–CN axis. This indicated the possible origin of sediments from plagioclase mineral-bearing source rocks, mainly the granites and gneisses. The samples belonging to the late Miocene and the Pliocene were plotted above the upper continental crust (UCC) and altered Post-Archaean Australian Shale (PAAS) values, indicating the possible intense weathering of felsic rocks. On the other hand, the Pleistocene (excluding the time period from 1.9 to 1.2 Ma) sediments fall close to basalt rocks, indicating the possible origin of sediments from basaltic rocks.

The major-element (Fe/Al, Mg/Al, Ti/Al), trace-element (Cr/Al, Co/Al), chondrite-normalized rare earth element (La/Sm)_N and published isotopic proxy data (Cai *et al.* 2019; Zhou *et al.* 2021) from IODP Sites U1457 and U1456 have been used to decipher the sediment provenance in the NE Arabian Sea (Figs 3 and 6). In general, the K/Al, Mg/Al and Fe/Al values indicate relative depletion of mobile elements in sediments during weathering (Nesbitt & Markovics, 1980). However, these geochemical proxies are influenced by sediment provenance, degree of chemical alteration and hydraulic sediment sorting (Fralick & Kronberg, 1997; Wan *et al.* 2017). Therefore, these geochemical proxies should be carefully analysed for possible control of weathering, provenance and hydraulic sorting (Wan *et al.* 2017). The major elements (e.g. K, Mg, Fe and Al) are enriched in clay minerals. The retention of these elements depends on mineral phases and their specific grain size (Nath *et al.* 2005; Wan *et al.* 2017). In particular, K is enriched in illite rather than in smectite while Mg and Fe are enriched in chlorite and smectite (Wan *et al.* 2017; Cai *et al.* 2020). The values of Mg/Al and Fe/Al are proportionally related to the relative abundance of smectite content within the

clay mineral assemblage. On the other hand, compatible elements such as Cr, Co and Sm are preferentially associated with early crystallized magmatic minerals (mafic) while the La is associated with later crystallized felsic minerals. The Al-normalized elemental ratios of trace metals (Cr and Co) and chondrite-normalized rare earth element ratio (La/Sm)_N could be used to decipher the sediment provenance in the marine sediments.

At Site U1457, the elemental ratios show statistically insignificant correlation with mean grain size, suggesting negligible role of hydraulic sorting. Therefore, these geochemical proxies could be used to track the sediment provenance and weathering conditions in the catchment area. The Indus River-supplied Himalayan sediment is rich in illite and smectite (Rao & Rao, 1995; Kessarkar *et al.* 2003; Alizai *et al.* 2012), and the Peninsular River-supplied Deccan Trap sediment is rich in smectite (Debrabant *et al.* 1991; Rao & Rao, 1995; Kessarkar *et al.* 2003; Phillips *et al.* 2014). Therefore, the K/Al (associated with illite), Mg/Al and Fe/Al (associated with smectite), Cr/Al (associated with primary mafic minerals) and La/Sm _N (relative dominance of felsic to mafic mineral source) values were used in this study to decipher the Himalayan and Deccan Province sediment in the NE Arabian Sea. At Site U1457, the elemental composition of sediment does not show significant variation during the late Miocene (Fig. 3). The sediment composition was characterized by low Mg/Al, Fe/Al, Cr/Al and high K/Al and (La/Sm)_N indicating homogeneous felsic sedimentary source, possibly derived from the Indus River. On the other hand, the elemental ratios show an increase in Mg/Al, Fe/Al, Cr/Al, Co/Al and decrease in K/Al and (La/Sm)_N during the late Pleistocene (between 1.2 and 0.25 Ma), which suggests possible dominance of primitive igneous source rock derived sediments (Fig. 3).

The sediments derived through primitive igneous rocks (mafic rocks) exhibit higher magnetic mineral concentration due to the presence of Fe-oxides, and mineralogy is expected to be dominated by magnetite and titanomagnetite (Rao & Wagle, 1997; Kumar *et al.* 2005; Sangode *et al.* 2017; Sebastian *et al.* 2019). The magnetic susceptibility is generally the result of sediment provenance, sediment grain size and sediment diagenesis. At Site U1457, the effect of sediment grain size and early diagenesis was minimal (see Section 5.a), and thus, magnetic susceptibility was found to be largely controlled by sediment provenance. The mafic source rocks are more prone to weathering than felsic rocks under similar morphoclimatic settings (Dupré *et al.* 2003; Gurumurthy *et al.* 2012). At Site U1457, the higher magnetic mineral concentration (high χ_{lf} , χ_{ARM} and SIRM), high detritus (ARF %) and magnetite–titanomagnetite mineralogy (S-ratio > 0.9) coincided with low (La/Sm)_N and high Mg/Al and Fe/Al values, suggesting dominance of mafic magnetic mineral sources during the Pleistocene (Figs 2 and 3). This observation is consistent with previous studies suggesting changes in provenance during the Pleistocene (Cai *et al.* 2019; Yu *et al.* 2019; Carter *et al.* 2020). The felsic and mafic source rock sediments have distinct χ_{lf} and SIRM signatures. The positive correlation between χ_{lf} and SIRM of sediments from Site U1457 reflects felsic source rock magnetic signatures. However, few samples belonging to the Pleistocene exhibit mafic source rock magnetic signatures (higher χ_{lf} and SIRM). These samples exhibit higher S-ratio, interparametric ratio (high $\chi_{\text{ARM}}/\chi_{\text{lf}}$) and the presence of magnetite–titanomagnetite (Fig. 4). Further, the χ –T curves and remnant coercivity (H_{cr}) measurements of the selected samples with suspected mafic rock contribution reflected the presence of magnetite and haematite mineral phases during the Quaternary and the late Miocene time period (Figs 4 and 5c–f), suggesting the two possible mineral sources at the study site.

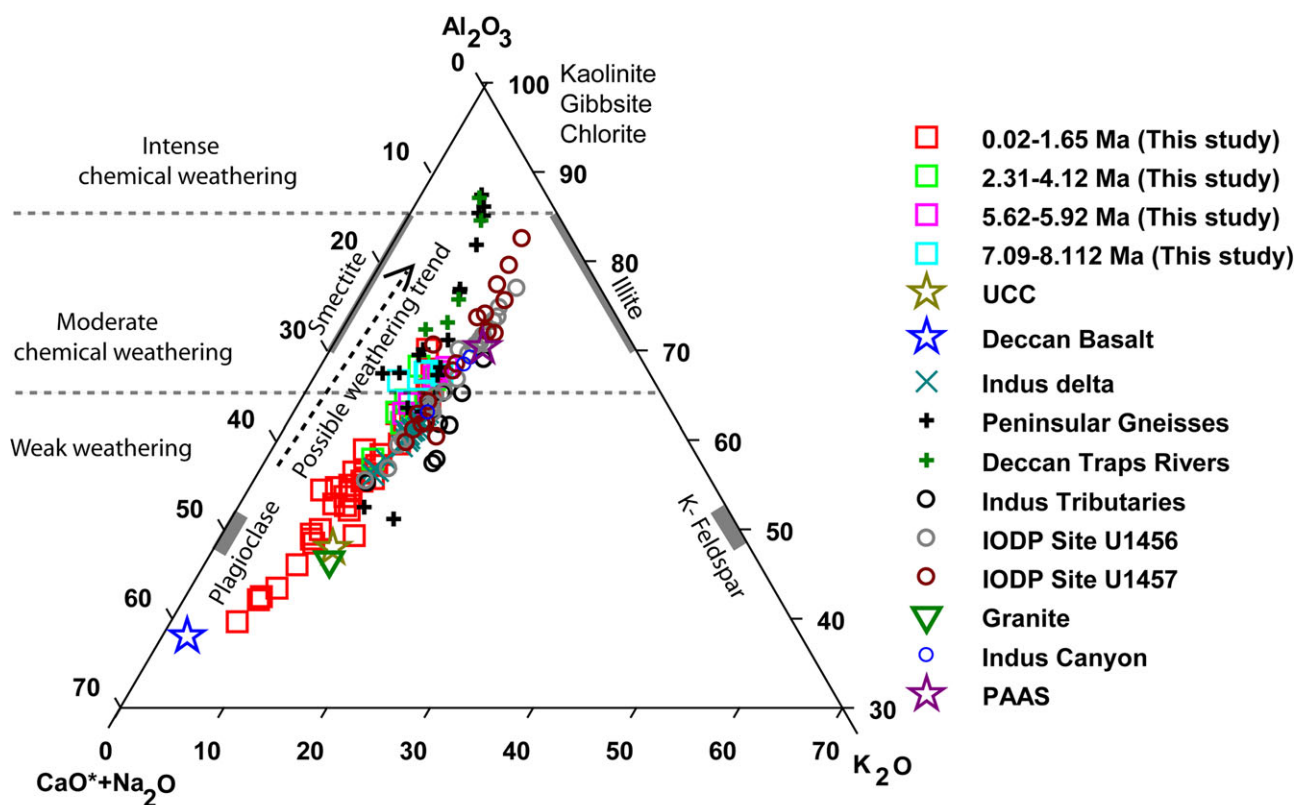


Fig. 6. (Colour online) Geochemical parameters plotted for provenance discrimination diagram. The A–CN–K plot suggests the sediment mainly derived through the Indus River (granitic composition) with minor contribution from Narmada, Tapi (Deccan basalt). Geochemical data is compared with existing studies on the Indus catchment: Indus tributaries (Alizai *et al.* 2011); Indus canyon (Li *et al.* 2018); Indus delta (Clift *et al.* 2010); Peninsular gneisses and Deccan Traps rivers (Kurian *et al.* 2013); granite (Sharma & Rajamani, 2000); Deccan basalt (Peng *et al.* 1994); upper continental crust (UCC) and Post-Archaean Australian Shale (PAAS) (Taylor & McLennan, 1985); IODP Site U1457 and U1456 (Zhou *et al.* 2021). For interpretation of the references to colour in the legend, the reader is referred to the web version of this article.

However, the environmental study can be useful for inferring sediment source at Site U1457.

Interestingly, at Site U1457, higher values of the χ_{If} and SIRM with titanomagnetite–magnetite were also observed during the late Miocene and Pliocene, which pointed to a possible mafic rock sediment provenance. The Deccan basalt / Trans-Himalayan mafic rocks generally exhibit positive ϵ_{Nd} values, and sedimentary and plutonic rocks of the Indus River exhibit negative ϵ_{Nd} values (Clift *et al.* 2002b, Clift, 2006). The negative ϵ_{Nd} values, smectite clay mineralogy and slightly lower ratios of $(La/Sm)_N$, Fe/Al , Cr/Al and Co/Al are observed during the high humid climatic phases. However, these elemental ratios and ϵ_{Nd} values are slightly intermediate between felsic and mafic composition. The intermediate sediment geochemical composition could emanate when there is mixing of mafic and felsic source sediments. Though the Indus River Basin is dominantly of felsic composition, the Trans-Himalayan region of the western Himalayas is composed of mafic lithology. The weathering and erosion of Indus River Basin rocks (felsic as well as mafic) could lead to intermediate composition with slight mafic bias.

5.d. Erosion and monsoon since the late Miocene

Silicate weathering intensity and erosional records have been useful in reconstructing the monsoon in the South Asian region. On a global scale, the warm temperature and high surface runoff lead to intense silicate weathering (West *et al.* 2005; Gurusurthy *et al.* 2012) and erosion (Gaillardet *et al.* 1999; Millot *et al.* 2003).

The dependence of weathering and erosion processes on the hydroclimate (runoff and temperature), lithology and geomorphology has been the basis for using sedimentary archives for palaeoclimate reconstruction of different geological timescales (West *et al.* 2005; Lara *et al.* 2018).

The silicate weathering, erosion and sedimentation pattern at Site U1457 of the Laxmi Basin show high temporal variation since the late Miocene, implying changes in hydroclimatic conditions in the drainage area. At Site U1457, the sedimentary and geochemical record shows moderate chemical weathering and low detrital supply during the late Miocene, except for the period between 7.6–7.5 Ma and 6.0–5.6 Ma where high clastic sedimentation (high LMAR) is observed. The high clastic sedimentation during 7.6–7.5 Ma at Site U1457 is also characterized by coarse sediment grains and higher magnetic susceptibility (Weber *et al.* 2003; Reilly *et al.* 2020). The geochemical data suggests an increase in altered sediment supply at 7.0 Ma implying humid climatic conditions, while the environmental magnetic and sediment texture data does not reflect humid climatic conditions in the region. An additional dataset is needed to ascertain the hydroclimatic conditions at 7 Ma. Therefore, this study infers that the long-term trend in hydroclimatic conditions in the Indus River Basin during the late Miocene is relatively drier except for the period from 6.0 to 5.6 Ma. The long-term drying with decline in the monsoon during the late Miocene is consistent with the global cooling. In contrast, the high sedimentation rate (high LMAR) during 6.0–5.6 Ma is associated with altered sediments having fluctuating clay–silt sediments and low magnetic susceptibility (Fig. 4). These sediments are

deposited in a distal setting of the fan (Clift *et al.* 2020). The humid climatic conditions during 6.0 to 5.6 Ma induced chemical alteration of sediments, and enhanced erosion of continental rocks, suggesting that the sediments are produced under transport-limited conditions. The chemically altered sediments (CIA, low K/Al and Mg/Al), elevated clastic flux (high Ti/Al) and high sedimentation rate (LMAR) were observed during the time interval 6.0–5.6 Ma (Fig. 3). Further, a coarsening of grain size possibly under high-energy conditions and higher detrital sediments was also observed for the same time interval. The environmental magnetic characteristics such as increased magnetic mineral concentration (i.e. high χ_{lf} , X_{ARM} and SIRM), finer to coarser magnetic grain size (i.e. low interparametric ratio, χ_{ARM}/χ_{lf}), and high proportion of magnetite relative to haematite mineral (i.e. S-ratio > 0.9) are also consistent with geochemical and sedimentological observations (Fig. 4). These observations suggest moderate alteration of the sediments with higher erosion in the catchment under transport-limited conditions during 6.0–5.6 Ma.

As discussed earlier, the Pliocene sedimentary record of Site U1457 is primarily composed of redeposited turbidites derived from the Indus. An exception to this is hemipelagic sediments belonging to the depth range 500–530 m (age 4.12 to 3.4 Ma; discussed in Section 5.c). The mid-Pliocene hemipelagic sediments of Site U1457 (depth range 500–530 m; age 4.12 to 3.4 Ma) show intense silicate weathering indicating humid climatic conditions (Fig. 3). The humid hydroclimatic conditions during the mid-Pliocene (4.12 to 3.4 Ma) could be inferred from the proxy record of increase in chemical weathering (high CIA and lower K/Al) and higher clastic flux (increased ARF %, Ti/Al ratio, and a corresponding increase in LMAR). Further, the higher magnetic concentration, magnetic mineralogy (dominated by haematite relative to magnetite) and magnetic grain size (finer to coarser) in the mid-Pliocene sediment record suggest humid hydroclimatic conditions (Fig. 4). The formation of permanent ice caps in the northern hemisphere (Raymo, 1994; Zhang *et al.* 2009), caused by tectonically induced changes in oceanic gateways, played an important role in strengthening the ISM. The mid-Pliocene witnessed worldwide changes in palaeoceanography, possibly driven by the tectonic rearrangement of seaways, and subsequent blockage of the heat transfer among the world oceans, thus altering the thermocline structure of the Indo-Pacific Ocean (Karas *et al.* 2009, 2011, 2017; Nie *et al.* 2014; Herbert *et al.* 2016).

The Pleistocene sedimentary record (Figs 3 and 4) of the NE Arabian Sea at Site U1457 shows an overall increase in mean grain size, enhanced detrital supply (high ARF % and Ti/Al) and high magnetic mineral content (high χ_{lf}) with dominance of magnetite mineralogy (S-ratio > 0.9). However, during the same period, the chemical weathering is observed to be moderate (relatively lower values of CIA* and higher values of K/Al). These proxy signatures indicate an increase in the physical weathering and low–moderate chemical weathering in the catchment. The Pleistocene sediment exhibits enhanced physical erosion with higher detrital supply to Site U1457, particularly during the interglacial periods (Khim *et al.* 2020a). These proxies suggest that the moisture content during the Pleistocene is variable, and the interplay between monsoon and weathering affects the sediment provenance (Kulkarni *et al.* 2015; Badesab *et al.* 2021). In particular, the interglacial or strengthened summer monsoon period shows highly altered sediments from the Indus region with additional input from the Deccan basalts. On the other hand, sediments during the glacial periods of the Pleistocene are less altered and are transported from the Indus River Basin.

Within the Pleistocene, the timespan 1.8–1.2 Ma shows a significant increase in sedimentation rate (high LMAR but low to moderate detrital flux), and intense chemical weathering (K/Al and CIA = 69–78) indicating either enhanced erosion under humid climatic conditions or enhanced recycling through the Indus River system. For the same period, the environmental magnetic data shows low magnetic mineral concentration (i.e. low χ_{ARM} , χ_{lf} and SIRM) with coarser magnetic grains (i.e. reduced χ_{ARM}/χ_{lf}) and magnetic mineralogy dominated by haematite (S-ratio < 0.9). Interestingly, in spite of glacial and interglacial conditions, the above time period shows relatively lower variability in proxy signatures, suggesting a relatively homogeneous sediment source and shift in hydroclimatic conditions during the Pleistocene. The interval 1.8–1.2 Ma also witnessed a high rate of sedimentation in the eastern Arabian Sea. The high sedimentation rate is interpreted as turbidite deposits (Pandey *et al.* 2016), and these deposits contain terrestrial organic matter dominated by C-3 plants (Khim *et al.* 2020b). A recent study suggested that the strengthening of winter monsoon and the weakening of summer monsoon favour the growth of C-3 vegetation (Basu *et al.* 2019). The changes in Arabian Sea surface hydrography and productivity induced by the strengthening of the winter monsoon were reported earlier for the same period (1.8–1.6 Ma; Satpathy *et al.* 2020). Therefore, it is possible that the strengthened winter monsoon during 1.8–1.2 Ma has brought altered sediments through the Indus River to Site U1457 of the Laxmi Basin.

The change in lithofacies and textural characteristics at depth 74.4 mbsf (~1.2 Ma) of site U1457 (transition in lithofacies from Unit II to Unit I) is interpreted as a result of lateral migration depocentre or dynamics of the channel levee system (Pandey *et al.* 2016). However, transition from Unit II to Unit I is also associated with a shift in sediment provenance from Indus-dominated sediments to Deccan-basalt-dominated sediments. Dominance of mafic sediment provenance is inferred for the period from 1.2 to 0.25 Ma based on an overall enrichment of major and trace elements, smectite clay mineralogy and radiogenic ϵ_{Nd} values (discussed in Section 5c). For the same period, the chemical alteration of sediments has reduced (low CIA and higher K/Al), suggesting weaker monsoon conditions in the region. The weaker monsoon in the Indus catchment is also reported from Site U1456 for the period from 1.1 to 0.1 Ma (Lu *et al.* 2020). The migration of the ITCZ from northern to southern latitudes shifts the rainfall distribution towards the peninsular region, leading to weathering of Deccan Province in Peninsular India. Therefore, the monsoon strength is likely to exhibit significant control over the Indus Fan sedimentation. Thus, the geochemical and environmental magnetic characterization of sediments from Site U1457 in the NE Arabian Sea demonstrates the link between monsoon strength and erosion over the Indian subcontinent since the late Miocene.

6. Conclusions

The link between the erosional history of the western Himalayas and the ISM evolution since the late Miocene has been explored in this study using marine sediment records from the Indus Fan in the NE Arabian Sea at Site U1457 of the Laxmi Basin collected during IODP Expedition 355. The geochemical, environmental magnetic and sedimentological signatures of the NE Arabian Sea sediments indicated that the climatic condition in the western Himalayas during the late Miocene was predominantly arid, except for the humid interval from 6.1 to 5.6 Ma. The mid-Pliocene and the Pleistocene climate in the western Himalayas were observed to

be humid. The climatic condition during the mid-Pleistocene period (1.9 Ma–1.2 Ma) was observed to be intensely humid. The observed cyclicity in the measured proxies during the Pleistocene suggested variability in the moisture content during its sedimentation which further coincided with the glacial and interglacial moisture variability. The study indicated that the dominant source of sediment in the NE Arabian Sea at Site U1457 during the late Miocene and the Pliocene was the Indus River while the Pleistocene sediments had characteristics of mixed sources derived from the Indus River and the western Indian Peninsular Rivers. This study revealed that the sediments of Site U1457 in the NE Arabian Sea were derived additionally from the Deccan basalts during the weaker summer monsoonal conditions of the Pleistocene (1.2 to 0.25 Ma).

Supplementary material. To view supplementary material for this article, please visit <https://doi.org/10.1017/S0016756822001273>

Acknowledgements. This work is funded by IODP-India and NCPOR, Goa under the Post-Cruise Research Funding Scheme (Grant No. NCAOR/IODP/20-15/15(V)) to GPG. Dr Vandana Prasad (Director, BSIP), Dr Anupam Sharma (Senior Scientist, BSIP) and Dr Binita Phartiyal (Senior Scientist, BSIP) are thanked for support and encouragement at various stages of this work. GPG thank the Indian National Science Academy (INSA) for the award of the ‘Establishment of Young Researcher – 2018’ fellowship under the INSA–JSPS bilateral Program. TM thanks the INSA and the Department of Science and Technology (DST) for the INSPIRE Faculty fellowship. The authors acknowledge JOIDES RESOLUTION, the International Ocean Discovery Program (IODP), Dr Denise K Kulhanek (Expedition Manager) and all shipboard scientists and crew members of the IODP-355 expedition for their support during sample collection. TR acknowledges the support from the Council of Scientific and Industrial Research (CSIR) for Emeritus Scientist (Grant No. 21(1041)/2017/EMR -II). The authors thank Prof. Peter D Clift (Editor-in-Chief), and three anonymous reviewers for their constructive comments on the initial version of the manuscript. This is BSIP contribution No. 55/2020-2021.

Conflict of interest. None.

References

- Alam M, Tripti M, Gurumurthy GP, Sohrin Y, Tsujisaka M, Singh AD, Takano S and Verma K (2022) Palaeoredox reconstruction in the eastern Arabian Sea since late Miocene: insights from trace element and stable isotopes of molybdenum ($\delta^{98/95}\text{Mo}$) and tungsten ($\delta^{186/184}\text{W}$) at the IODP Site U1457 of Laxmi basin. *Palaeogeography, Palaeoclimatology, Palaeoecology* **587**, 110790. <https://doi.org/10.1016/j.palaeo.2021.110790>
- Alizai A, Carter A, Clift PD, Van Laningham S, Williams JC and Kumar R (2011) Sediment provenance, reworking and transport processes in the Indus River by U–Pb dating of detrital zircon grains. *Global and Planetary Change* **76**, 33–55. <https://doi.org/10.1016/j.gloplacha.2010.11.008>
- Alizai A, Hillier S, Clift PD, Giosan L, Hurst A, Van Laningham S and Macklin M (2012) Clay mineral variations in Holocene terrestrial sediments from the Indus Basin. *Quaternary Research* **77**, 368–81. <https://doi.org/10.1016/j.yqres.2012.01.008>
- Amano K and Taira A (1992) Two-phase uplift of Higher Himalayas since 17 Ma. *Geology* **20**, 391–4. [https://doi.org/10.1130/0091-7613\(1992\)020<0391:TPUOHH>2.3.CO;2](https://doi.org/10.1130/0091-7613(1992)020<0391:TPUOHH>2.3.CO;2)
- An Z, Kutzbach JE, Prell WL and Porter SC (2001) Evolution of Asian monsoons and phased uplift of the Himalaya–Tibetan Plateau since late Miocene times. *Nature* **411**, 62–6.
- Badesab F, Gaikwad V, Nath BN, Venkateshwarlu M, Aiswarya PV, Tyagi A, Salunke K, Fernandes W, Kadam N, Sangode SJ, Sardar A and Prabhu G (2021) Controls of contrasting provenance and fractionation on the sediment magnetic records from the Bay of Bengal. *Marine Geology* **437**, 106515. <https://doi.org/10.1016/j.palaeo.2013.04.012>
- Banse K (1987) Seasonality of phytoplankton chlorophyll in the central and northern Arabian Sea. *Deep Sea Research Part A. Oceanographic Research Papers* **34**, 713–23. [https://doi.org/10.1016/0198-0149\(87\)90032-X](https://doi.org/10.1016/0198-0149(87)90032-X)
- Basu S, Ghosh S and Sanyal P (2019) Spatial heterogeneity in the relationship between precipitation and carbon isotopic discrimination in C3 plants: inferences from a global compilation. *Global and Planetary Change* **176**, 123–31. <https://doi.org/10.1016/j.gloplacha.2019.02.002>
- Berner RA (1981) A new geochemical classification of sedimentary environments. *Journal of Sedimentary Research* **51**, 359–65. <https://doi.org/10.1306/212F7C7F-2B24-11D7-8648000102C1865D>
- Betzler C, Eberli GP, Kroon D, Wright JD, Swart PK, Nath BN, Alvarez-Zarikian CA, Alonso-Garcia M, Bialik OM, Blatter CL, Gua JA, Haffien S, Horozal S, Inoue M, Jovane L, Lanci L, Laya JC, Hui-Mee AL, Ludmann T, Nakakuni M, Niino K, Petruny LM, Pratiwi SD, Reijmer JGG, Reolid, J, Slagle AL, Sloss CR, Xiang S, Yao Z and Young JR (2016) The abrupt onset of the modern South Asian Monsoon winds. *Scientific Report* **6**, 29838. <https://doi.org/10.1038/srep29838>
- Blott SJ and Pye K (2001) GRADISTAT: a grain size distribution and statistics package for the analysis of unconsolidated sediments. *Earth Surface Processes and Landforms* **26**, 1237–48. <https://doi.org/10.1002/esp.261>
- Brock J, Sathyendranath S and Platt T (1994) A model study of seasonal mixed-layer primary production in the Arabian Sea. *Proceedings of the Indian Academy of Sciences – Earth and Planetary Sciences* **103**, 163–76. <https://doi.org/10.1007/BF02839534>
- Cai M, Xu Z, Clift PD, Khim BK, Lim D, Yu Z, Kulhanek DK and Li T (2020) Long-term history of sediment inputs to the eastern Arabian Sea and its implications for the evolution of the Indian summer monsoon since 3.7 Ma. *Geological Magazine* **157**, 908–19. <https://doi.org/10.1017/S0016756818000857>
- Cai M, Xu Z, Clift PD, Lim D, Khim BK, Yu Z, Kulhanek DK, Li T, Chen H and Sun R (2019) Depositional history and Indian summer monsoon controls on the silicate weathering of sediment transported to the eastern Arabian Sea: geochemical records from IODP Site U1456 since 3.8 Ma. *Geochemistry, Geophysics, Geosystems* **20**, 43396–4353. <https://doi.org/10.1029/2018GC008157>
- Canfield DE and Thamdrup BO (2009) Towards a consistent classification scheme for geochemical environments, or, why we wish the term ‘suboxic’ would go away. *Geobiology* **7**, 385–92. <https://doi.org/10.1111/j.1472-4669.2009.00214.x>
- Carter SC, Griffith EM, Clift PD, Scher HD and Dellapenna TM (2020) Clay-fraction strontium and neodymium isotopes in the Indus Fan: implications for sediment transport and provenance. *Geological Magazine* **157**, 879–94. <https://doi.org/10.1017/S0016756820000394>
- Carter SC, Griffith EM, Scher HD and the Expedition 355 Scientists (2017) Data report: 87Sr/86Sr in pore fluids from IODP Expedition 355 Arabian Sea Monsoon. In Pandey, D.K., Clift, P.D., Kulhanek, D.K., and the Expedition 355 Scientists, Arabian Sea Monsoon. Proceedings of the International Ocean Discovery Program, 355: College Station, TX (International Ocean Discovery Program). <https://doi.org/10.14379/iodp.proc.355.201.201>
- Chen H, Xu Z, Clift PD, Lim D, Khim BK and Yu Z (2019) Orbital-scale evolution of the Indian summer monsoon since 1.2 Ma: evidence from clay mineral records at IODP Expedition 355 Site U1456 in the eastern Arabian Sea. *Journal of Asian Earth Sciences* **174**, 11–22. <https://doi.org/10.1016/j.jseas.2018.10.012>
- Cheng H, Zhang PZ, Spötl C, Edwards RL, Cai YJ, Zhang DZ, Sang WC, Tan M and An, ZS (2012) The climatic cyclicity in semiarid-arid central Asia over the past 500,000 years. *Geophysical Research Letters* **39**, L01705. <https://doi.org/10.1029/2011GL050202>
- Clark DA and Emerson DW (1991) Notes on rock magnetization characteristics in applied geophysical studies. *Exploration Geophysics* **22**, 547–55. <https://doi.org/10.1071/EG991547>
- Clemens S, Prell W, Murray D, Shimmield G and Weedon G (1991) Forcing mechanisms of the Indian Ocean monsoon. *Nature* **353**, 720–5.
- Clemens SC and Prell WL (2003) A 350,000 year summer-monsoon multiproxy stack from the Owen Ridge, Northern Arabian Sea. *Marine Geology* **201**, 35–51. [https://doi.org/10.1016/S0025-3227\(03\)00207-X](https://doi.org/10.1016/S0025-3227(03)00207-X)

- Clift PD (2006) Controls on the erosion of Cenozoic Asia and the flux of clastic sediment to the ocean. *Earth and Planetary Science Letters* **241**, 571–80. <https://doi.org/10.1016/j.epsl.2005.11.028>
- Clift PD and Blusztajn J (2005) Reorganization of the western Himalayan river system after five million years ago. *Nature* **438**, 1001–3. <https://doi.org/10.1038/nature04379>
- Clift PD, Carter A, Draut AE, Van Long H, Chew DM and Schouten HA (2009) Detrital U–Pb zircon dating of lower Ordovician Syn-Arc-continent collision conglomerates in the Irish Caledonides. *Tectonophysics* **479**, 165–74. <https://doi.org/10.1016/j.tecto.2008.07.018>
- Clift PD, Giosan L, Carter A, Garzanti E, Galy V, Tabrez AR and Rabbani MM (2010) Monsoon control over erosion patterns in the western Himalaya: possible feed-back into the tectonic evolution. In *Monsoon Evolution and Tectonics–Climate Linkage in East Asia* (ed. PD Clift), pp. 185–218. Geological Society of London, Special Publication no. 342. <https://doi.org/doi:10.1144/SP342.12>
- Clift PD, Hodges KV, Heslop D, Hannigan R., Van Long H and Calves G (2008) Correlation of Himalayan exhumation rates and Asian monsoon intensity. *Nature Geoscience* **1**, 875. <https://doi.org/10.1038/ngeo0351>
- Clift PD, Kulhanek DK, Zhou P, Bowen MG, Vincent SM, Lyle M and Hahn A (2020) Chemical weathering and erosion responses to changing monsoon climate in the Late Miocene of Southwest Asia. *Geological Magazine* **157**, 939–55. <https://doi.org/10.1017/S0016756819000608>
- Clift PD, Kroon D, Gaedicke C and Craig J (eds) (2002a) The tectonic and climatic evolution of the Arabian Sea region. In *Quaternary Climates, Environments and Magnetism* (eds BA Maher and R Thompson). Geological Society of London, Special Publication no. 195, 1–5. <https://doi.org/10.1017/S0016756803278833>
- Clift PD, Lee JL, Hildebrand P, Shimizu N, Layne GD, Blusztajn J, Blum JD, Garzanti E and Khan AA (2002b) Nd and Pb isotope variability in the Indus River System: implications for sediment provenance and crustal heterogeneity in the Western Himalaya. *Earth and Planetary Science Letters* **200**, 91–106. [https://doi.org/10.1016/S0012-821X\(02\)00620-9](https://doi.org/10.1016/S0012-821X(02)00620-9)
- Clift PD, Shimizu N, Layne GD, Blusztajn JS, Gaedicke C, Schluter HU and Amjad S (2001) Development of the Indus Fan and its significance for the erosional history of the Western Himalaya and Karakoram. *Geological Society of America Bulletin* **113**, 1039–51. <https://doi.org/10.1017/S0016756818000857>
- Clift PD, Wan S and Blusztajn J (2014) Reconstructing chemical weathering, physical erosion and monsoon intensity since 25 Ma in the northern South China Sea: a review of competing proxies. *Earth-Science Reviews* **130**, 86–102. <https://doi.org/10.1016/j.earscirev.2014.01.002>
- Clift PD and Webb AG (2019) A history of the Asian monsoon and its interactions in Cenozoic, South Asia. In *Himalayan Tectonics: A Modern Synthesis* (eds PJ Treloar and MP Searle), pp. 631–52. Geological Society of London, Special Publication no. 483. <https://doi.org/10.1144/SP483.1>
- Clift PD, Zhou P, Stockli DF and Blusztajn JS (2019b) Regional Pliocene exhumation of the Lesser Himalaya in the Indus drainage. *Solid Earth* **10**, 647–61. <https://doi.org/10.5194/se-10-647-2019>
- Davies TA, Kidd RB and Ramsay AT (1995) A time-slice approach to the history of Cenozoic sedimentation in the Indian Ocean. *Sedimentary Geology* **96**, 157–79. [https://doi.org/10.1016/0037-0738\(94\)00131-D](https://doi.org/10.1016/0037-0738(94)00131-D)
- Dearing JA (1999) *Holocene environmental change from magnetic proxies in lake sediments*. In *Quaternary Climates, Environments and Magnetism*, pp. 231–78. Cambridge: Cambridge University Press. <https://doi.org/10.1017/CBO9780511535635>
- Debrabant P, Krissek L, Bouquillon A and Chamley H (1991) Clay mineralogy of Neogene sediments of the western Arabian Sea: mineral abundances and paleoenvironmental implications. In *Proceedings of the Ocean Drilling Program, Scientific Results, Vol. 117* (eds WL Prell and N Niitsuma), pp. 183–96. College Station, Texas.
- Dillon M and Bleil U (2006) Rock magnetic signatures in diagenetically altered sediments from the Niger deep-sea fan. *Journal of Geophysical Research: Solid Earth* **111**. <https://doi.org/10.1029/2004JB003540>
- Dunlo DJ and Özdemir Ö (1997) *Rock Magnetism: Fundamentals and Frontiers*. New York: Cambridge University Press, 573 pp.
- Dupré B, Dessert C, Oliva P, Goddéri Y, Viers J, François L, Millot R and Gaillardet J (2003) Rivers, chemical weathering and Earth's climate. *Comptes Rendus Geoscience* **335**, 1141–60. <https://doi.org/10.1016/j.crte.2003.09.015>
- Evans M and Heller F (eds) (2003) *Environmental Magnetism: Principles and Applications of Enviromagnetics*. Amsterdam: Elsevier.
- Farnsworth A, Lunt DJ, Robinson SA, Valdes PJ, Roberts WH, Clift PD, Markwick P, Su T, Wrobel N, Bragg F and Kelland SJ (2019) Past East Asian monsoon evolution controlled by paleogeography, not CO₂. *Science Advances* **30**, 5, eaax1697. <https://www.science.org/doi/10.1126/sciadv.aax1697>
- Feakins, SJ, Liddy HM, Tauxe L, Galy V, Feng X, Tierney JE, Miao Y and Warny S (2020) Miocene C4 grassland expansion as recorded by the Indus Fan. *Paleoceanography and Paleoclimatology* **35**, e2020PA003856. <https://doi.org/10.1029/2020PA003856>
- Fedo CM, Nesbitt W and Young GM (1995) Unraveling the effects of potassium metasomatism in sedimentary rocks and paleosols, with implications for paleoweathering conditions and provenance. *Geology* **23**, 921–4. [https://doi.org/10.1130/0091-7613\(1995\)023<0921:UTEOPM>2.3.CO;2](https://doi.org/10.1130/0091-7613(1995)023<0921:UTEOPM>2.3.CO;2)
- Fralick PW and Kronberg BI (1997) Geochemical discrimination of clastic sedimentary rock sources. *Sedimentary Geology* **113**, 111–24. [https://doi.org/10.1016/S0037-0738\(97\)00049-3](https://doi.org/10.1016/S0037-0738(97)00049-3)
- France-Lanord C, Derry L and Michard A (1993) Evolution of the Himalaya since Miocene time: isotopic and sedimentological evidence from the Bengal Fan. In *Himalayan Tectonics* (ed. PJ Treloar), pp. 603–21. *Geological Society of London, Special Publication no. 74*. <https://doi.org/10.1144/GSL.SP.1993.074.01.40>
- Gaillardet J, Dupré B, Louvat P and Allegre CJ (1999) Global silicate weathering and CO₂ consumption rates deduced from the chemistry of large rivers. *Chemical Geology* **159**, 3–30. [https://doi.org/10.1016/S0009-2541\(99\)00031-5](https://doi.org/10.1016/S0009-2541(99)00031-5)
- Garming JF, Bleil U and Riedinger N (2005) Alteration of magnetic mineralogy at the sulfate–methane transition: analysis of sediments from the Argentine continental slope. *Physics of the Earth and Planetary Interiors* **151**, 290–308. <https://doi.org/10.1016/j.pepi.2005.04.001>
- Garzanti E, Baud A and Mascle G (1987) Sedimentary record of the northward flight of India and its collision with Eurasia (Ladakh Himalaya, India). *Geodinamica Acta* **1**, 297–312. <https://doi.org/10.1080/09853111.1987.11105147>
- Ghosh P, Padia JT and Mohindra R (2004) Stable isotopic studies of paleosol sediment from upper Siwalik of Himachal Himalaya: evidence for high monsoonal intensity during late Miocene. *Paleogeography, Palaeoclimatology, Palaeoecology* **206**, 103–14. <https://doi.org/10.1016/j.palaeo.2004.01.014>
- Gupta AK and Thomas E (2003) Initiation of Northern Hemisphere glaciation and strengthening of the northeast Indian monsoon: Ocean Drilling program site 758, eastern equatorial Indian Ocean. *Geology* **31**, 47–50. [https://doi.org/10.1130/0091-7613\(2003\)031<0047:IONHGA>2.0.CO;2](https://doi.org/10.1130/0091-7613(2003)031<0047:IONHGA>2.0.CO;2)
- Gupta AK, Yuvaraja A, Prakasam M, Clemens SC and Velu A (2015) Evolution of the South Asian monsoon wind system since the late Middle Miocene. *Paleogeography, Palaeoclimatology, Palaeoecology* **438**, 160–7. <https://doi.org/10.1016/j.palaeo.2015.08.006>
- Gurumurthy GP, Balakrishna K, Riotte J, Braun JJ, Audry S, Shankar HU and Manjunatha BR (2012) Controls on intense silicate weathering in a tropical river, southwestern India. *Chemical Geology* **300**, 61–9. <https://doi.org/10.1016/j.chemgeo.2012.01.016>
- Herbert TD, Lawrence KT, Tzanova A, Peterson LC, Caballero-Gill R and Kelly CS (2016) Late Miocene global cooling and the rise of modern ecosystems. *Nature Geoscience* **9**, 843–7. [10.1038/ngeo2813](https://doi.org/10.1038/ngeo2813)
- Hodges KV (2000) Tectonics of the Himalaya and southern Tibet from two perspectives. *Geological Society of America Bulletin* **112**, 324–50. [https://doi.org/10.1130/0016-7606\(2000\)112<324:TOTHAS>2.0.CO;2](https://doi.org/10.1130/0016-7606(2000)112<324:TOTHAS>2.0.CO;2)
- Holbourn AE, Kuhnt W, Clemens SC, Kochhann KGD, Johnk J, Lubbers J and Andersen N, (2018) Late Miocene climate cooling and intensification of southeast Asian winter monsoon. *Nature Communication* **9**, 1584. <https://doi.org/10.1038/s41467-018-03950-1>
- Karas C, Nürnberg D, Bahr A, Groeneveld J, Herrle JO, Tiedemann R and Demenocal PB (2017) Pliocene oceanic seaways and global climate. *Scientific Reports* **7**, 1–8. [10.1038/srep39842](https://doi.org/10.1038/srep39842)

- Karas C, Nürnberg D, Gupta AK, Tiedemann R, Mohan K and Bickert T** (2009) Mid-Pliocene climate change amplified by a switch in Indonesian subsurface throughflow. *Nature Geoscience* **2**, 434–8. <https://doi.org/10.1038/ngeo520>
- Karas C, Nürnberg D, Tiedemann R and Garbe-Schönberg D** (2011) Pliocene Indonesian throughflow and Leeuwin Current dynamics: implications for Indian Ocean polar heat flux. *Paleoceanography* **26**. PA2217. [10.1029/2010PA001949](https://doi.org/10.1029/2010PA001949)
- Karim A and Veizer J** (2002) Water balance of the Indus River Basin and moisture source in the Karakoram and western Himalayas: implications from hydrogen and oxygen isotopes in river water. *Journal of Geophysical Research: Atmospheres* **107**, ACH-9. <https://doi.org/10.1029/2000>
- Kessarkar PM, Rao VP, Ahmad SM and Babu GA** (2003) Clay minerals and Sr–Nd isotopes of the sediments along the western margin of India and their implication for sediment provenance. *Marine Geology* **202**, 55–69. [https://doi.org/10.1016/S0025-3227\(03\)00240-8](https://doi.org/10.1016/S0025-3227(03)00240-8)
- Khim BK, Horikawa K, Asahara Y, Kim JE and Ikehara M** (2020a) Detrital Sr–Nd isotopes, sediment provenances and depositional processes in the Laxmi Basin of the Arabian Sea during the last 800 ka. *Geological Magazine* **157**, 895–907. <https://doi.org/10.1017/S0016756818000596>
- Khim BK, Lee J, Ha S, Park J, Pandey DK, Clift PD, Kulhanek DK, Steinke S, Griffith EM, Suzuki K and Xu Z** (2020b) Variations in $\delta^{13}\text{C}$ values of sedimentary organic matter since late Miocene time in the Indus Fan (IODP Site 1457) of the eastern Arabian Sea. *Geological Magazine* **157**, 1012–21. <https://doi.org/10.1017/S0016756818000870>
- King JW and Channell JE** (1991) Sedimentary magnetism, environmental magnetism, and magnetostratigraphy. *Reviews of Geophysics* **29**, 358–70. <https://doi.org/10.1002/rog.1991.29.s1.358>
- Kroon D, Steens T and Troelstra SR** (1991) Onset of monsoon related upwelling in the western Arabian Sea as revealed by planktonic foraminifers. *Proceedings of the Ocean Drilling Program, Scientific Results* **117**, 257–63. [10.2973/odp.proc.sr.117.126.1991](https://doi.org/10.2973/odp.proc.sr.117.126.1991)
- Kulkarni YR, Sangode SJ, Bloemendal J, Meshram DC and Suresh N** (2015) Mineral magnetic characterization of the Godavari River and western Bay of Bengal sediments: Implications to source to sink relations. *Journal of the Geological Society of India* **85**, 71–8. <https://doi.org/10.1007/s12594-015-0194-7>
- Kumar AA, Rao VP, Patil SK, Kessarkar PM and Thamban M** (2005) Rock magnetic records of the sediments of the eastern Arabian Sea: evidence for late Quaternary climatic change. *Marine Geology* **220**, 59–82. <https://doi.org/10.1016/j.margeo.2005.06.038>
- Kumar PS, Narvekar J, Kumar A and Shaji C** (2004) Intrusion of the Bay of Bengal water into the Arabian Sea during winter monsoon and associated chemical and biological response. *Geophysical Research Letters* **31**, L15304. [10.1029/2004GL020247](https://doi.org/10.1029/2004GL020247)
- Kurian S, Nath BN, Kumar NC and Nair KKC** (2013) Geochemical and isotopic signatures of surficial sediments from the western continental shelf of India: inferring provenance, weathering, and the nature of organic matter. *Journal of Sedimentary Research* **83**, 427–42. [10.2110/jsr.2013.36](https://doi.org/10.2110/jsr.2013.36)
- Lara MC, Buss HL and Pett-Ridge JC** (2018) The effects of lithology on trace element and REE behavior during tropical weathering. *Chemical Geology* **500**, 88–102. <https://doi.org/10.1016/j.chemgeo.2018.09.024>
- Li Y, Clift PD, Böning P, Blusztajn J, Murray RW, Ireland T and Giosan L** (2018) Continuous Holocene input of river sediment to the Indus Submarine Canyon. *Marine Geology* **406**, 159–76. <https://doi.org/10.1016/j.margeo.2018.09.011>
- Licht A, Van Cappelle M, Abels HA, Ladant JB, Trabucho-Alexandre J, France-Lanord C, Donnadiu Y, Vandenberghe J, Rigaudier T, Lecuyer C, Terry Jr, Adriaens R, Boura A, Guo, G, Anung NS, Quade J, Dupont-Nivet G and Jaeger JJ** (2014) Asian monsoons in a late Eocene greenhouse world. *Nature* **513**, 501–506. <https://doi.org/10.1038/nature13704>
- Liu J, Zhu R, Roberts AP, Li S and Chang JH** (2004) High-resolution analysis of early diagenetic effects on magnetic minerals in post-middle-Holocene continental shelf sediments from the Korea Strait. *Journal of Geophysical Research: Solid Earth* **109**. <https://doi.org/10.1029/2003JB002813>
- Lu, H., Liu, R., Cheng, L., Feng, H., Zhang, H., Wang, Y, Hu R, Zhao W, Ji J, Xu Z, Yu Z, Kulhanek DK, Pandey DK and Clift, PD** (2020) Phased evolution and variation of the South Asian monsoon, and resulting weathering and surface erosion in the Himalaya–Karakoram Mountains, since late Pliocene time using data from Arabian Sea core. *Geological Magazine* **157**, 864–78. <https://doi.org/10.1017/S0016756820000291>
- Luis AJ and Kawamura H** (2004) Air-sea interaction, coastal circulation and primary production in the eastern Arabian Sea: a review. *Journal of Oceanography* **60**, 205–18. <https://doi.org/10.1023/B:JOCE.0000038327.33559.34>
- Lupker M, France-Lanord C, Galy V, Lavé J and Kudrass H** (2013) Increasing chemical weathering in the Himalayan system since the Last Glacial Maximum. *Earth and Planetary Science Letters* **365**, 243–52. [10.1016/j.epsl.2013.01.038](https://doi.org/10.1016/j.epsl.2013.01.038)
- Maher BA** (1988) Magnetic properties of some synthetic sub-micron magnetites. *Geophysical Journal* **94**, 83–96. <https://doi.org/10.1111/j.1365-246X.1988.tb03429.x>
- Maher BA and Thompson R** (1992) Paleoclimatic significance of the mineral magnetic record of the Chinese loess and paleosols. *Quaternary Research* **37**, 155–70. [https://doi.org/10.1016/0033-5894\(92\)90079-X](https://doi.org/10.1016/0033-5894(92)90079-X)
- Milliman JD and Syvitski PM** (1992) Geomorphic/tectonic control of sediment discharge to the ocean: the importance of small mountainous rivers. *The Journal of Geology* **100**, 525–44. <https://doi.org/10.1086/629606>
- Millot R, Gaillardet J, Dupré B and Allègre CJ** (2003) Northern latitude chemical weathering rates: clues from the Mackenzie River Basin, Canada. *Geochimica et Cosmochimica Acta* **67**, 1305–29. [https://doi.org/10.1016/S0016-7037\(02\)01207-3](https://doi.org/10.1016/S0016-7037(02)01207-3)
- Molnar P** (1984) Structure and tectonics of the Himalaya: constraints and implications of geophysical data. *Annual Reviews in Earth and Planetary Sciences* **12**, 489–518. <https://doi.org/10.1146/annurev.ea.12.050184.002421>
- Molnar P** (2004) Late Cenozoic increase in accumulation rates of terrestrial sediment: how might climate change have affected erosion rates. *Annual Reviews in Earth and Planetary Sciences* **32**, 67–89. <https://doi.org/10.1146/annurev.earth.32.091003.143456>
- Molnar P, Boos WR and Battisti DS** (2010) Orographic controls on climate and paleoclimate of Asia: thermal and mechanical roles for the Tibetan Plateau. *Annual Review of Earth and Planetary Sciences* **38**, 77–102. <https://doi.org/10.1146/annurev-earth-040809-152456>
- Molnar P and Tapponnier P** (1978) Active tectonics of Tibet. *Journal of Geophysical Research: Solid Earth* **83**, 5361–75. <https://doi.org/10.1029/JB083iB11p05361>
- Mugnier JL and Huyghe P** (2006) The Ganges basin geometry records a pre-15Ma isostatic rebound of Himalaya. *Geology* **34**, 445–8. <https://doi.org/10.1130/G22089.1>
- Mungekar TV, Naik SS, Nath NB and Pandey DK** (2020) Shell weights of foraminifera trace atmospheric CO₂ from the Miocene to Pleistocene in the central Equatorial Indian Ocean. *Journal of Earth System Science* **129**, 69. <https://doi.org/10.1007/s12040-020-1348-6>
- Nath BN, Gupta SM, Mislankar PG, Rao BR, Parthiban G, Roelandts I and Patil SK** (2005) Evidence of Himalayan erosional event at ~0.5 Ma from a sediment core from the equatorial Indian Ocean in the vicinity of ODP Leg 116 sites. *Deep Sea Research Part II: Topical Studies in Oceanography* **52**, 2061–77. <https://doi.org/10.1016/j.dsr2.2005.05.011>
- Nesbitt HW and Markovics G** (1980) Chemical processes affecting alkalis and alkaline earths during continental weathering. *Geochimica et Cosmochimica Acta* **44**, 1659–66. [https://doi.org/10.1016/0016-7037\(80\)90218-5](https://doi.org/10.1016/0016-7037(80)90218-5)
- Nesbitt HW and Young GM** (1984) Prediction of some weathering trends of plutonic and volcanic rocks based on thermodynamic and kinetic considerations. *Geochimica et Cosmochimica Acta* **48**, 1523–34. [https://doi.org/10.1016/0016-7037\(84\)90408-3](https://doi.org/10.1016/0016-7037(84)90408-3)
- Nie J, Stevens T, Song Y, King JW, Zhang R, Ji S, Gong L and Cares D** (2014) Pacific freshening drives Pliocene cooling and Asian monsoon intensification. *Scientific Reports* **4**. <https://doi.org/10.1038/srep05474>
- Oldfield F** (1991) Environmental magnetism: a personal perspective. *Quaternary Science Reviews* **10**, 73–85. [https://doi.org/10.1016/0277-3791\(91\)90031-O](https://doi.org/10.1016/0277-3791(91)90031-O)
- Pandey DK, Clift PD, Kulhanek DK, Andò S, Bendle JAP, Bratenkov S, Griffith EM, Gurumurthy GP, Hahn A, Iwai M, Khim, BK, Kumar A, Kumar AG, Liddy HM, Lu H, Lyle MW, Mishra R, Radhakrishna T,**

- Routledge CM, Saraswat R, Saxena R, Scardia G, Sharma GK, Singh AD, Steinke S, Suzuki K, Tauxe L, Tiwari M, Xu Z and Yu Z (2016) Expedition 355 summary. In *Proceedings of the International Ocean Discovery Program, 355* (eds DK Pandey, PD Clift, DK Kulhanek and the Expedition 355 Scientists, Arabian Sea Monsoon). College Station, Texas: International Ocean Discovery Program. <https://doi.org/10.14379/iodp.proc.355.101.2016>
- Pandey OP, Agrawal PK and Negi JG (1995) Lithospheric structure beneath Laxmi Ridge and late Cretaceous geodynamic events. *Geo-Marine Letters* **15**, 85–91. <https://doi.org/10.1007/BF01275411>
- Peng ZX, Mahoney J, Hooper P, Harris C and Beane J (1994) A role for lower continental crust in flood basalt genesis? Isotopic and incompatible element study of the lower six formations of the western Deccan Traps. *Geochimica et Cosmochimica Acta* **58**, 267–88. [https://doi.org/10.1016/0016-7037\(94\)90464-2](https://doi.org/10.1016/0016-7037(94)90464-2)
- Phillips SC, Johnson JE, Underwood MB, Guo J, Giosan L and Rose K (2014) Long-timescale variation in bulk and clay mineral composition of Indian continental margin sediments in the Bay of Bengal, Arabian Sea, and Andaman Sea. *Marine and Petroleum Geology* **58**, 117–38. <https://doi.org/10.1016/j.marpetgeo.2014.06.018>
- Prell WL, Murray DW, Clemens SC and Anderson DM (1992) Evolution and variability of the Indian Ocean summer monsoon: evidence from the western Arabian Sea drilling program. *Washington DC American Geophysical Union Geophysical Monograph Series* **70**, 447–69. <https://doi.org/10.1029/GM070p0447>
- Quade J and Cerling TE (1995) Expansion of C4 grasses in the late Miocene of northern Pakistan: evidence from stable isotopes in paleosols. *Palaeogeography, Palaeoclimatology, Palaeoecology* **115**, 91–116. [https://doi.org/10.1016/0031-0182\(94\)00108-K](https://doi.org/10.1016/0031-0182(94)00108-K)
- Quade J, Cerling TE and Bowman JR (1989) Development of Asian monsoon revealed by marked ecological shift during the latest Miocene in northern Pakistan. *Nature* **342**, 163. <https://doi.org/10.1038/342163a0>
- Rao VP and Rao BR (1995) Provenance and distribution of clay minerals in the sediments of the western continental shelf and slope of India. *Continental Shelf Research* **15**, 1757–71. [https://doi.org/10.1016/0278-4343\(94\)00092-2](https://doi.org/10.1016/0278-4343(94)00092-2)
- Rao VP and Wagle BG (1997) Geomorphology and surficial geology of the western continental shelf and slope of India: a review. *Current Science* **73**, 330–50.
- Raymo ME (1994) The initiation of Northern Hemisphere glaciation. *Annual Review of Earth and Planetary Sciences* **22**, 353–83.
- Reilly BT, Bergmann F, Weber ME, Stoner JS, Selkin P, Meynadier L, Schwenk T, Spiess V and France-Lanord C (2020) Middle to late Pleistocene evolution of the Bengal Fan: integrating core and seismic observations for chronostratigraphic modeling of the IODP Expedition 354 8 north transect. *Geochemistry, Geophysics, Geosystems* **21**, e2019GC008878. <https://doi.org/10.1029/2019GC008878>
- Roberts AP (2015) Magnetic mineral diagenesis. *Earth-Science Reviews* **151**, 1–47. <https://doi.org/10.1016/j.earscirev.2015.09.010>
- Routledge CM, Kulhanek DK, Tauxe L, Scardia G, Singh AD, Steinke S, Griffith EM and Saraswat R (2019) A revised chronostratigraphic framework for International Ocean Discovery Program Expedition 355 sites in Laxmi basin, eastern Arabian Sea. *Geological Magazine* **157**, 961–78. <https://doi.org/10.1017/S0016756819000104>
- Sangode SJ, Sharma R, Mahajan R, Basavaiah N, Srivastava P, Gudadhe SS, Meshram DC and Venkateshwarulu M (2017) Anisotropy of magnetic susceptibility and rock magnetic applications in the Deccan volcanic province based on some case studies. *Journal of the Geological Society of India* **89**, 631–42.
- Satpathy RK, Steinke S and Singh AD (2020) Monsoon-induced changes in surface hydrography of the eastern Arabian Sea during the early Pleistocene. *Geological Magazine* **157**, 1001–11. <https://doi.org/10.1017/S0016756819000098>
- Schott F (1983) Monsoon response of the Somali Current and associated upwelling. *Progress in Oceanography* **12**, 357–81. [https://doi.org/10.1016/0079-6611\(83\)90014-9](https://doi.org/10.1016/0079-6611(83)90014-9)
- Searle MP (1996) Cooling history, erosion, exhumation and kinematics of the Himalaya–Karakoram–Tibet orogenic belt. In *The Tectonic Evolution of Asia* (eds A Yin and TM Harrison), pp. 110–37. Cambridge: Cambridge University Press.
- Sebastian T, Nath BN, Ramaswamy V, Mascarenhas-Pereira MBL, Yazing AK, Apurva PR, Linsy P, Kocherla P, Miriyala P and Rao BR (2019) Distribution and dispersal of surface sediments on the continental margins of India. *Marine and Petroleum Geology* **110**, 122–37. <https://doi.org/10.1016/j.marpetgeo.2019.07.017>
- Sharma A and Rajamani V (2000) Weathering of gneissic rocks in the upper reaches of Cauvery River, south India: implications to neotectonics of the region. *Chemical Geology* **166**, 203–23. [https://doi.org/10.1016/S0009-2541\(99\)00222-3](https://doi.org/10.1016/S0009-2541(99)00222-3)
- Shetye SR, Gouveia AD, Shenoi SSC, Michael GS, Sundar D, Almeida AM and Santanam K (1991) The coastal current off western India during the northeast monsoon. *Deep Sea Research Part A. Oceanographic Research Papers* **38**, 1517–1529. [https://doi.org/10.1016/0198-0149\(91\)90087-V](https://doi.org/10.1016/0198-0149(91)90087-V)
- Singh M, Sharma M and Tobschall HJ (2005) Weathering of the Ganga alluvial plain, northern India: implications from fluvial geochemistry of the Gomati River. *Applied Geochemistry* **20**, 1–21. <https://doi.org/10.1016/j.apgeochem.2004.07.005>
- Stober JC and Thompson R (1979) An investigation into the source of magnetic minerals in some Finnish lake sediments. *Earth and Planetary Science Letters* **45**, 464–474. <https://doi.org/10.1029/91JB03068>
- Stoner JS, Channell JE and Hillaire-Marcel C (1996) The magnetic signature of rapidly deposited detrital layers from the deep Labrador Sea: relationship to North Atlantic Heinrich layers. *Paleoceanography* **11**, 309–325. <https://doi.org/10.1029/96PA00583>
- Tada R, Zheng H and Clift PD (2016) Evolution and variability of the Asian monsoon and its potential linkage with uplift of the Himalaya and Tibetan Plateau. *Progress in Earth and Planetary Science* **3**, 4. <https://doi.org/10.1186/s40645-016-0080-y>
- Taylor SR and McLennan SM (1985) *The Continental Crust: Its Composition and Evolution*. Oxford: Blackwell, 312 pp. <https://doi.org/10.1002/gj.3350210116>
- Thompson R and Oldfield F (1986) *Environmental Magnetism*. London: Allen and Unwin.
- Thomson JR, Holden PB, Anand P, Edwards NR, Porchier CA and Harris NBW (2021) Tectonic and climatic drivers of Asian monsoon evolution. *Nature Communications* **12**, 4022. <https://doi.org/10.1038/s41467-021-24244-z>
- Tripathy GR, Singh SK and Ramaswamy V (2014) Major and trace element geochemistry of Bay of Bengal sediments: implications to provenances and their controlling factors. *Palaeogeography, Palaeoclimatology, Palaeoecology* **397**, 20–30. <https://doi.org/10.1016/j.palaeo.2013.04.012>
- Verosub KL and Roberts AP (1995) Environmental magnetism: past, present, and future. *Journal of Geophysical Research: Solid Earth* **100**, 2175–92. <https://doi.org/10.1029/94JB02713>
- Walden J, Smith JP and Oldfield F (eds) (1999) *Environmental Magnetism: A Practical Guide*. London: Quaternary Research Association. Technical Guide, no. 6.
- Walden J (1999) Remanence measurements. In *Environmental Magnetism: A Practical Guide* (eds J Walden, JP Smith and F Oldfield), pp. 63–88. London: Quaternary Research Association. Technical Guide, no. 6.
- Wan S, Clift PD, Zhao D, Hovius N, Munhoven G, France-Lanord C, Wang Y, Xiong A, Huang J, Yu Z, Zhnag J, Wentao M, Zhang G, Li A and Li T (2017) Enhanced silicate weathering of tropical shelf sediments exposed during glacial lowstands: a sink for atmospheric CO₂. *Geochimica et Cosmochimica Acta* **200**, 123–144. <https://doi.org/10.1016/j.gca.2016.12.010>
- Wang P, Clemens S, Beaufort L, Braconnot P, Ganssen G, Jian Z, Kershaw P and Sarnthein, M. (2005) Evolution and variability of the Asian monsoon system: state of the art and outstanding issues. *Quaternary Science Reviews* **24**, 595–629. <https://doi.org/10.1016/j.quascirev.2004.10.002>
- Weber ME, Wiedicke-Hombach M, Kudrass HR and Erlenkeuser H (2003) Bengal Fan sediment transport activity and response to climate forcing inferred from sediment physical properties. *Sedimentary Geology* **155**, 361–81. [https://doi.org/10.1016/S0037-0738\(02\)00187-2](https://doi.org/10.1016/S0037-0738(02)00187-2)

- Weltje GJ and von Eynatten H** (2004) Quantitative provenance analysis of sediments: review and outlook. *Sedimentary Geology* **171**, 1–11. <https://doi.org/10.1016/j.sedgeo.2004.05.007>
- West AJ, Galy A and Bickle M** (2005) Tectonic and climatic controls on silicate weathering. *Earth and Planetary Science Letters* **235**, 211–28. <https://doi.org/10.1016/j.epsl.2005.03.020>
- Yu Z, Colin C, Wan S, Saraswat R, Song L, Xu Z, Clift P, Lu H, Lyle M, Kulhanek D, Hahn A, Tiwari M, Mishra R, Miska S and Kumar A** (2019) Sea level-controlled sediment transport to the eastern Arabian Sea over the past 600 kyr: clay minerals and Sr–Nd isotopic evidence from IODP site U1457. *Quaternary Science Reviews* **205**, 22–34. <https://doi.org/10.1016/j.quascirev.2018.12.006>
- Zhang GJ, Song X and Wang Y** (2019) The double ITCZ syndrome in GCMs: a coupled feedback problem among convection, clouds, atmospheric and ocean circulations. *Atmospheric Research* **229**, 255–268. <https://doi.org/10.1016/j.atmosres.2019.06.023>
- Zhang YG, Ji J, Balsam W, Liu L and Chen J** (2009) Mid-Pliocene Asian monsoon intensification and the onset of Northern Hemisphere glaciation. *Geology* **37**, 599–602. <https://doi.org/10.1130/G25670A.1>
- Zhisheng A, Guoxiong W, Jianping L, Youbin S, Yimin L, Weijian Z, Yanjun C, Anmin D, Li L, Jiangyu M and Hai C** (2015) Global monsoon dynamics and climate change. *Annual Review of Earth and Planetary Sciences* **43**, 29–77. <https://doi.org/10.1146/annurev-earth-060313-054623>
- Zhou P, Ireland T, Murray RW and Clift PD** (2021) Marine sedimentary records of chemical weathering evolution in the western Himalaya since 17 Ma. *Geosphere* **17**, 824–853. <https://doi.org/10.1130/GES02211.1>